ISSN 1948-0210 (online)

World Journal of *Stem Cells*

World J Stem Cells 2024 October 26; 16(10): 854-899

Published by Baishideng Publishing Group Inc

WJSC

World Journal of Stem Cells

Contents

Monthly Volume 16 Number 10 October 26, 2024

World Journal of Stem Cells

Monthly Volume 16 Number 10 October 26, 2024

Contents

ABOUT COVER

Editorial Board Member of *World Journal of Stem Cells*, Konstantinos I Papadopoulos, MD, PhD, Chairman, Chief Doctor, Director, Department of Research and Development, THAI StemLife, Bangkok 10310, Thailand. kostas@thaistemlife.co.th

AIMS AND SCOPE

The primary aim of *World Journal of Stem Cells* (*WJSC*, *World J Stem Cells*) is to provide scholars and readers from various fields of stem cells with a platform to publish high-quality basic and clinical research articles and communicate their research findings online. *WJSC* publishes articles reporting research results obtained in the field of stem cell biology and regenerative medicine, related to the wide range of stem cells including embryonic stem cells, germline stem cells, tissue-specific stem cells, adult stem cells, mesenchymal stromal cells, induced pluripotent stem cells, embryonal carcinoma stem cells, hemangioblasts, lymphoid progenitor cells, *etc*.

INDEXING/ABSTRACTING

The *WJSC* is now abstracted and indexed in Science Citation Index Expanded (SCIE, also known as SciSearch®), Journal Citation Reports/Science Edition, PubMed, PubMed Central, Scopus, Biological Abstracts, BIOSIS Previews, Reference Citation Analysis, China Science and Technology Journal Database, and Superstar Journals Database. The 2024 Edition of Journal Citation Reports® cites the 2023 journal impact factor (JIF) for *WJSC* as 3.6; JIF without journal self cites: 3.5; 5-year JIF: 4.2; JIF Rank: 105/205 in cell biology; JIF Quartile: Q3; and 5-year JIF Quartile: Q2. The *WJSC*'s CiteScore for 2023 is 7.8 and Scopus CiteScore rank 2023: Histology is 11/62; Genetics is 78/347; Genetics (clinical) is 19/99; Molecular Biology is 131/410; Cell Biology is 104/285.

RESPONSIBLE EDITORS FOR THIS ISSUE

Production Editor: *Wen-Bo Wang*; **Production Department Director:** *Xu Guo*; **Cover Editor:** *Jia-Ru Fan*.

NAME OF JOURNAL
World Journal of Stem Cells

ISSN
ISSN 1948-0210 (online)

LAUNCH DATE
December 31, 2009

FREQUENCY
Monthly

EDITORS-IN-CHIEF
Shengwen Calvin Li, Carlo Ventura

EDITORIAL BOARD MEMBERS
https://www.wjgnet.com/1948-0210/editorialboard.htm

PUBLICATION DATE
October 26, 2024

INSTRUCTIONS TO AUTHORS
https://www.wjgnet.com/bpg/gerinfo/204

GUIDELINES FOR ETHICS DOCUMENTS
https://www.wjgnet.com/bpg/GerInfo/287

GUIDELINES FOR NON-NATIVE SPEAKERS OF ENGLISH
https://www.wjgnet.com/bpg/gerinfo/240

PUBLICATION ETHICS
https://www.wjgnet.com/bpg/GerInfo/288

PUBLICATION MISCONDUCT
https://www.wjgnet.com/bpg/gerinfo/208

ARTICLE PROCESSING CHARGE
https://www.wjgnet.com/bpg/gerinfo/242

STEPS FOR SUBMITTING MANUSCRIPTS
https://www.wjgnet.com/bpg/GerInfo/239

ONLINE SUBMISSION
https://www.f6publishing.com

World Journal of Stem Cells

Submit a Manuscript: https://www.f6publishing.com

World J Stem Cells 2024 October 26; 16(10): 873-895

DOI: 10.4252/wjsc.v16.i10.873

ISSN 1948-0210 (online)

ORIGINAL ARTICLE

Basic Study

Gamma-aminobutyric acid enhances miR-21-5p loading into adipose-derived stem cell extracellular vesicles to alleviate myocardial ischemia-reperfusion injury *via* TXNIP regulation

Feng-Dan Wang, Yi Ding, Jian-Hong Zhou, En Zhou, Tian-Tian Zhang, Yu-Qi Fan, Qing He, Zong-Qi Zhang, Cheng-Yu Mao, Jun-Feng Zhang, Jing Zhou

Specialty type: Cell and tissue engineering

Provenance and peer review: Unsolicited article; Externally peer reviewed.

Peer-review model: Single blind

Peer-review report's classification

Scientific Quality: Grade B, Grade B, Grade C, Grade C

Novelty: Grade B, Grade B, Grade C

Creativity or Innovation: Grade B, Grade B, Grade C

Scientific Significance: Grade B, Grade B, Grade C

P-Reviewer: Eid N; Li SC; Li WJ

Received: April 1, 2024

Revised: August 21, 2024

Accepted: September 27, 2024

Published online: October 26, 2024

Processing time: 206 Days and 11.4 Hours

Feng-Dan Wang, Jian-Hong Zhou, En Zhou, Tian-Tian Zhang, Yu-Qi Fan, Qing He, Zong-Qi Zhang, Cheng-Yu Mao, Jun-Feng Zhang, Jing Zhou, Department of Cardiology, Shanghai Ninth People's Hospital, Shanghai Jiao Tong University School of Medicine, Shanghai 200011, China

Yi Ding, Department of Anesthesiology, Shanghai Ninth People's Hospital, Shanghai Jiao Tong University School of Medicine, Shanghai 200011, China

Co-first authors: Feng-Dan Wang and Yi Ding.

Co-corresponding authors: Jing Zhou and Cheng-Yu Mao.

Corresponding author: Jing Zhou, MM, Doctor, Teacher, Department of Cardiology, Shanghai Ninth People's Hospital, Shanghai Jiao Tong University School of Medicine, No. 280 Mohe Road, Baoshan District, Shanghai 200011, China. zj9hospital@163.com

Abstract

BACKGROUND

Myocardial ischemia-reperfusion injury (MIRI) poses a prevalent challenge in current reperfusion therapies, with an absence of efficacious interventions to address the underlying causes.

AIM

To investigate whether the extracellular vesicles (EVs) secreted by adipose mesenchymal stem cells (ADSCs) derived from subcutaneous inguinal adipose tissue (IAT) under γ-aminobutyric acid (GABA) induction (GABA-EVs^{IAT}) demonstrate a more pronounced inhibitory effect on mitochondrial oxidative stress and elucidate the underlying mechanisms.

METHODS

We investigated the potential protective effects of EVs derived from mouse ADSCs pretreated with GABA. We assessed cardiomyocyte injury using terminal deoxynucleotidyl transferase dUTP nick end-labeling and Annexin V/propidium iodide assays. The integrity of cardiomyocyte mitochondria morphology was assessed using electron microscopy across various intervention backgrounds. To explore the functional RNA diversity between EVs^{IAT} and GABA-EVs^{IAT}, we em-

ployed microRNA (miR) sequencing. Through a dual-luciferase reporter assay, we confirmed the molecular mechanism by which EVs mediate thioredoxin-interacting protein (TXNIP). Western blotting and immunofluorescence were conducted to determine how TXNIP is involved in mediation of oxidative stress and mitochondrial dysfunction.

RESULTS

Our study demonstrates that, under the influence of GABA, ADSCs exhibit an increased capacity to encapsulate a higher abundance of miR-21-5p within EVs. Consequently, this leads to a more pronounced inhibitory effect on mitochondrial oxidative stress compared to EVs from ADSCs without GABA intervention, ultimately resulting in myocardial protection. On a molecular mechanism level, EVs regulate the expression of TXNIP and mitigating excessive oxidative stress in mitochondria during MIRI process to rescue cardiomyocytes.

CONCLUSION

Administration of GABA leads to the specific loading of miR-21-5p into EVs by ADSCs, thereby regulating the expression of TXNIP. The EVs derived from ADSCs treated with GABA effectively ameliorates mitochondrial oxidative stress and mitigates cardiomyocytes damage in the pathological process of MIRI.

Key Words: Extracellular vesicles; Myocardial ischemia-reperfusion injury; Adipose-derived mesenchymal stem cells; Gamma-aminobutyric acid; Thioredoxin-interacting protein

Core Tip: Extracellular vesicles secreted by adipose mesenchymal stem cells derived from subcutaneous inguinal adipose tissue under γ-aminobutyric acid induction demonstrate a pronounced inhibitory effect on mitochondrial oxidative stress and showcases a safeguarding impact on the cardiomyocytes. The protective effects may result from extracellular vesicle microRNA-21-5p targeting thioredoxin (TXNIP)-interacting protein, regulating TXNIP-interacting protein-TXNIP complex formation and subsequent enhancing the antioxidant activity of TXNIP.

Citation: Wang FD, Ding Y, Zhou JH, Zhou E, Zhang TT, Fan YQ, He Q, Zhang ZQ, Mao CY, Zhang JF, Zhou J. Gamma-aminobutyric acid enhances miR-21-5p loading into adipose-derived stem cell extracellular vesicles to alleviate myocardial ischemia-reperfusion injury *via* TXNIP regulation. *World J Stem Cells* 2024; 16(10): 873-895

URL: https://www.wjgnet.com/1948-0210/full/v16/i10/873.htm

DOI: https://dx.doi.org/10.4252/wjsc.v16.i10.873

INTRODUCTION

Myocardial infarction (MI) is a grave cardiovascular ailment triggered by coronary occlusion, resulting in acute and persistent ischemia and hypoxia within the myocardium[1]. However, upon reestablishing blood flow to the previously occluded vessels, a phenomenon known as myocardial ischemia-reperfusion injury (MIRI) may occur, leading to potential secondary damage of the perfused myocardium, which continues to pose a significant challenge in clinical practice[2]. During the phase of MIRI, mitochondrial oxidative stress emerges as the predominant form of cardiomyocyte demise[3]. Hence, notwithstanding the expeditious reopening of occluded blood vessels and subsequent restoration of blood flow, the initial mitochondrial oxidative stress will further evolve into passive programmed cell death or even irreversible necrosis[4].

This culminates in an onslaught of mitochondrial oxidative stress, wherein excessive generation of mitochondrial reactive oxygen species (mROS) triggers a cascade of detrimental events, potentially compromising mitochondrial function[5,6]. Furthermore, heightened levels of mROS and hypoxia induce an upregulation of thioredoxin-interacting protein (TXNIP)[7], which impairs the resilience of cardiomyocytes to hypoxic conditions and incites mitochondrial oxidative stress which ultimately culminates in the collapse of mitochondrial membrane potential and functional impairment or even destruction, resulting in various programmed cell death events within cardiomyocytes after reperfusion therapy administration[8,9]. TXNIP impedes the reductive capacity of thioredoxin (TRX), thereby obstructing its function in regulating oxidative stress at both the cellular and subcellular levels with finesse[10]. Henceforth, targeting TXNIP emerges as a promising therapeutic strategy for safeguarding against MIRI encompassing mitochondrial oxidative stress triggered by hypoxia-oxygenation recovery arising from the restoration of blood flow[11-13].

Accumulating evidence has demonstrated that subcutaneous inguinal adipose tissue (IAT), particularly adipose-derived mesenchymal stem cells (ADSCs), possess remarkable regulatory functions regarding adipose tissue, peripheral organs, systemic inflammation, endoplasmic reticulum stress, and mitochondrial stress[14-16]. Moreover, these effects can be further augmented under the influence of γ-aminobutyric acid (GABA)[17]. The aforementioned biological effects are primarily believed to be mediated by extracellular vesicles (EVs), necessitating meticulous examination. EVs facilitate intercellular communication by transferring proteins, mRNAs, and microRNAs (miRs) in a manner that can be broad or

specific to certain cell types. The molecular composition of EVs reflects that of their source cells and can influence the biological functions of target cells, tissues, and organs such as differentiation, proliferation, migration, secretion, and apoptosis[18,19]. Changes in the microenvironment and physiological state of EV-producing cells can also impact both the contents and biological function of EVs[20,21]. Nevertheless, uncertainty persists regarding the role of EVs in mediating the GABA-induced impacts of ADSCs from IAT on mitigating mitochondrial dysfunction and oxidative stress. Moreover, a comprehensive exploration into the underlying mechanisms responsible for these effects is still pending.

The objective of this study was to investigate whether EVs derived from GABA-induced ADSCs from IAT (GABA-EVs^{IAT}) exert a more pronounced impact on ameliorating MIRI than EVs derived from ADSCs from IAT (EVs^{IAT}) and elucidate its underlying mechanisms to offer a potential efficacious approach for enhancing MIRI.

MATERIALS AND METHODS

MIRI mouse model

The Institutional Ethics Committee of Shanghai Ninth People's Hospital (Shanghai, China) granted proper approval for the animal care and procedures. The animal experimental protocols were meticulously followed in strict accordance with Directive 2010/63/EU. Male C57BL/6 mice, aged 8 weeks, were obtained from Shanghai Jessie Experimental Animal Co., Ltd. (Shanghai, China), and the establishment of transgenic mouse models was conducted by Shanghai Southern Model Organisms Co., Ltd. (Shanghai, China). These mice were provided with unrestricted access to standard mouse chow and water while being housed under specific pathogen-free conditions (maintained at a temperature range of 20-24 °C with humidity levels between 50% and 60%). All invasive procedures were conducted under anesthesia. Anesthesia induction was achieved using an anesthesia box infused with 2% isoflurane (RWD Life Technology Co., Ltd., Shenzhen, China) for 3 min, followed by maintenance anesthesia administered through an animal anesthetic mask containing a concentration of 1% isoflurane. Carbon dioxide inhalation was utilized as a humane method for euthanizing the mice. The traditional Cre-loxP system was used to construct all gene knockout (KO) mice, based on relevant research[22]. Cyagen Biotechnology Co., Ltd. (Jiangsu, China) and Shanghai Model Organisms Center, Inc. (Shanghai, China) completed the construction of all gene KO mice in this study.

A total of 80 male C57BL/6 mice, weighing between 20 g and 24 g, were employed for the experimental trials. We followed the detailed protocol outlined by Gao *et al*[23] to create the MI model. This involved 30 min of left coronary artery (LCA) ligation. Blood flow occlusion was temporarily induced using a slipknot and subsequently released to simulate reperfusion and restore blood supply to the ischemic regions. Successful confirmation of MI induction was based on dynamic electrocardiograph changes characterized by ST-segment elevation. As part of our control group, sham-operated mice underwent an identical procedure with the exception that the knot on the LCA remained loosely tied.

Transthoracic echocardiography

The echocardiography was conducted on the 3rd day post MIRI surgery, utilizing the state-of-the-art Vevo 770 high-resolution imaging system (FUJIFILM, Japan) in small animal models, to meticulously evaluate (M mode) ejection fraction and fractional shortening across three consecutive cardiac cycles.

Evaluation of area at risk and infarct size

After 12 h of MIRI, the LCA was re-ligated at the same level using a knot. Subsequently, under 1.5%-2% isoflurane anesthesia administration, the chest wall was reopened to elegantly expose the heart. Following this, meticulous reconnection of the LCA took place while gently applying a clamp to the aortic arch. Meanwhile, reverse injection of 1% Evans blue (dissolved in normal saline) through the ascending aorta resulted in non-infarcted areas displaying an exquisite blue coloration. Subsequently, with utmost care and precision, the heart was removed and rinsed with normal saline before being horizontally sliced into approximately 1 mm thick sections below the ligation level. Each section underwent immediate incubation in phosphate-buffered saline containing 1.5% triphenyltetrazolium chloride at 37 °C for 20 min. Utilizing Image-Pro Plus 6.0 software (Media Cybernetics, Inc., Rockville, MD, United States) with finesse and expertise, both the infarct area and area at risk (AAR) zone were quantified accordingly. The calculation involved determining infarct size/AAR × 100% as well as AAR/left ventricle area (LV) × 100%, respectively.

Isolation and culture of mouse ADSCs and neonatal mouse cardiomyocytes

The ADSCs were obtained from the IAT of C57BL/6 mice using a previously established protocol[24]. Flow cytometry analysis was conducted to characterize the ADSCs (Supplementary Figure 1), with a focus on cluster of differentiation 34 (CD34), CD105 (as negative controls), and CD106 as well as CD29, CD45, and CD90 (as positive cell surface markers). Primary neonatal mouse cardiomyocytes (NMCMs) were extracted from 1-day-old neonatal C57BL/6 mice and the protocol has been previously described[25].

In vitro cardiomyocyte hypoxia model

The creation of an *in vitro* NMCMs hypoxia model involved subjecting cells to a meticulously controlled environment devoid of oxygen and low in glucose, using DMEM. This was achieved by maintaining 5% CO_2 and 95% N_2 for a duration of 2 h. Subsequently, the incubation conditions were switched to normoxic fetal bovine serum (FBS)-free medium for 12 h. After treatment, the myocardial cells were collected and subjected to thorough analysis.

GABA-induced ADSCs

ADSCs were seeded in complete medium (DMEM/F12 with 10% EV-free FBS [EXO-FBS-50A-1; System Biosciences, Palo Alto, CA, United States]) for 24 h. The ADSCs were further cultured in a GABA-rich environment at a concentration of 5 μM, and the supernatant was collected for EV extraction after 48 h.

Isolation and characterization of EVs

The EVs were isolated from cultured ADSCs using differential velocity centrifugation[24], and the concentration of EVs was quantified using the bicinchoninic acid assay (BCA). Briefly, the cell culture supernatant was centrifuged at 2000 × *g* for 30 min at 4 °C to eliminate any cellular debris. Subsequently, the resulting supernatant was collected and further centrifuged at 100000 × *g* for 70 min to precipitate the EVs. To eliminate any contaminating proteins, the supernatant was discarded and the EVs were resuspended in phosphate-buffered saline (PBS). The size distribution and concentration of the EVs were determined utilizing the NanoSight NS300 instrument (Malvern Instruments, Malvern, United Kingdom), and their morphology was examined by transmission electron microscopy (TEM) and Nanosight.

EV injections and confirmation of EV uptake by cardiomyocytes

The EVs were injected into the border zone of the infarcted heart at three specific sites, immediately following MI surgery, at a dosage of 1 μg/1 g mouse body weight and the administered volume of EVs at each injection site was one-third of the total volume to be injected. These EVs were labeled with PKH67 (Cat. MINI67; Sigma-Aldrich, St. Louis, MO, United States), while the NMCMs were stained with phalloidin (Cat. A12379s; Thermo Fisher Scientific, Waltham, MA, United States). Each culture of NMCMs was treated with 20 μg EV solution (determined by the BCA), stained with 5 mL PKH67, and incubated for 2 h to facilitate endocytosis by the NMCMs. After being washed three times with PBS, the cells were fixed in 4% paraformaldehyde for 20 min and DAPI stain was used to label the nucleus. An inverted microscope was employed to observe the engulfed EVs within the cardiomyocytes.

Terminal deoxynucleotidyl transferase dUTP nick end-labeling assay

Sections were fixed in 4% paraformaldehyde for 15 min and then treated with 1 μg/mL proteinase K for 10-20 min. Then the sections were briefly refixed in 4% paraformaldehyde and washed twice with PBS for 5 min each. A positive control was prepared and excess liquid was removed from the slides. Next, 100 μL equilibration buffer was added to each slide, and the slides were carefully covered with plastic coverslips and incubated for 5-10 min. The plastic coverslips and excess buffer were carefully removed from the slides. TdT reaction mix (100 μL) or negative control (NC) mix was added instead of TdT reaction mix as a NC. Then the slides were carefully covered again with plastic coverslips and incubated at 37 °C for 1 h. The sections were washed three times with PBST for 10 min each before the slides were transferred to a slide rack. The sections were washed twice with dH_2O for 3 min each, followed by dehydration once in ethanol solutions (50%, 70%, 95%) and twice in pure ethanol (100%), with each step lasting 3 min. Then the sections were incubated twice in xylene for 3 min each before mounting slides using DPX and applying micro cover glasses while ensuring no air bubbles were trapped during this process.

Dual-luciferase reporter assay

HEK 293T cells were meticulously cultured in 24-well plates until they were approximately 70% confluent. Subsequently, a co-transfection was performed employing miR mimics and PGL3 luciferase plasmids harboring either wild-type, NC, or mutated TXNIP 3′ untranslated region (3′UTR) sequences. Following a 12-h incubation period, the cells were transferred to 96-well luciferase assay plates. Thereafter, the Dual-GLOTM Luciferase Assay System (Cat. E2920; Promega, Madison, WI, United States) was employed to determine the ratio of firefly to Renilla luciferase activity.

Oxygen consumption measurements

The Seahorse XFe96 Extracellular Flux Analyzer, in combination with the Seahorse Cell Mito Stress Test Kit (Agilent Technologies, Wilmington, DE, United States), were utilized to measure the oxygen consumption rates (OCRs) of NMCMs. The cells were cultured on Seahorse cell culture plates and subjected to the established protocol[26]. Prior to measurement, the culture media were replaced with Seahorse XF DMEM supplemented with 5 μM glucose, 1 μM pyruvate, and 10 μM glutamine for 1 h. Following incubation at 37 °C in a CO_2-free incubator for 1 h, the OCRs were assessed under both basal conditions and in the presence of oligomycin (1.5 mM), FCCP (1 mM), and rotenone/antimycin A (0.5 mM). To normalize the results, Hoechst 33342 staining was employed to determine total cell number at the conclusion of the Seahorse experiment.

Quantitative polymerase chain reaction and western blotting

We utilized the RNAiso Plus extraction reagent (Cat. 9108; Takara, Dalian, China) to isolate EV-associated RNA. To generate microRNA (miRNA) cDNA, we employed stem-loop primers from Ribobio Biotech and amplified the resulting cDNA using the SYBR Green-based quantitative polymerase chain (qPCR) reaction method. U6 small nuclear RNA was used as an internal control for normalization purposes. RIPA was implemented to extract protein from cardiac tissues and cardiomyocytes while antibodies against tumor susceptibility 101 (TSG101), CD63, CD81, thioredoxin-interacting protein (TXNIP) were obtained from Abcam (Cambridge, MA, United States) with α-tubulin antibodies provided by Cell Signaling Technology (Danvers, MA, United States).

TEM

To perform TEM, heart tissues were promptly immersed in 2.5% glutaraldehyde solution at 4 °C for fixation. The fixed samples underwent three rinses with a buffer containing 0.1 mM cacodylate trihydrate and were subsequently post-fixed using a solution of 1% osmium tetroxide for a duration of 1 h. Following three additional washes with PB, the samples were dehydrated through ethanol gradients, treated with acetone, and ultimately embedded in ethoxyline resin. Subsequently, ultrathin sections were carefully placed onto a copper grid before capturing images utilizing the FEI electron microscope (Tecnai G2 Spirit 120 kV; FEI Italia, Vercelli, Italy).

Statistical analysis

Data analysis was conducted utilizing the SPSS 19.0 software package (IBM Corp., Armonk, NY, United States). The assessment of normal distribution for the data was performed employing the Shapiro-Wilk test. Categorical variables were subjected to analysis using either the Pearson's χ^2 test (for $n \geq 5$) or Fisher's exact test (for $n < 5$), followed by multiple comparisons with Bonferroni correction. Continuous variables were analyzed with one-way analysis of variance, and subsequent post-hoc multiple comparisons were performed using the Student-Newman-Keuls test. Nonparametric testing for multiple independent samples was carried out utilizing the Kruskal-Wallis test, and post hoc comparisons were made with the Dunn-Bonferroni test.

RESULTS

Characterization of ADSCs and ADSC-derived EVs

A schematic diagram depicting the identification of ADSCs and the extraction of their EVs is presented in Figure 1A and B. The successful isolation of ADSCs from mouse adipose tissue was confirmed using flow cytometry, which showed that the cell surface markers CD29, CD45, and CD90 were expressed positively (> 80%), while CD34, CD105, and CD106 had low/negative expression (Supplementary Figure 1A). Sequential centrifugation was employed to obtain ADSC-derived EVs (ADSC-EVs), which then were characterized using TEM and the Nanosight instrument (Figure 1C and Supplementary Figure 1B). These analyses revealed that the collected vesicles primarily consisted of EVs with an average size of 115 nm (range: 50-150 nm). The EVs markers CD63, CD81, and TSG101 were identified by Western blotting (Supplementary Figure 1C). The uptake of PKH26-labeled EVs by cultured NMCMs was verified by fluorescence microscopy (Figure 1D).

GABA-EVs^{IAT} reduce injury in NMCMs subjected to hypoxia and reoxygenation

To investigate the potential of GABA-EVs^{IAT} in preventing or mitigating hypoxia and reoxygenation (H/R)-induced injury in NMCMs, injury-related markers were assessed using AnnexinV/PI (G1511; Servicebio, Wuhan, China) assay and terminal deoxynucleotidyl transferase dUTP nick end-labeling (TUNEL) assay (G1501; Servicebio) in NMCMs exposed to H/R (6 h of hypoxia followed by 12 h of reoxygenation) and treated with EVs^{IAT} or GABA-EVs^{IAT} prior to H/R. As demonstrated by the TUNEL assay results (Figure 1E), exposure to EVs^{IAT} reduced the apoptotic rate of NMCMs (P = 0.0035 for H/R + EVs^{IAT} *vs* H/R group). However, the downregulation of apoptosis was significantly greater after treatment with GABA-EVs^{IAT} (P = 0.0083 for H/R + GABA-EVs^{IAT} *vs* H/R + EVs^{IAT} group). Similarly, significant differences were observed in GABA-EVs^{IAT}-treated cells using AnnexinV/PI assay (P = 0.0009 for H/R + GABA-EVs^{IAT} *vs* H/R + EVs^{IAT} group) (Figure 1F).

GABA-EVs^{IAT} mitigates NMCMs mitochondrial oxidative stress levels and enhances mitochondrial function during H/R

The early pathogenesis of MIRI involves excessive mitochondrial oxidative stress as a pivotal mechanism[27]. We tried to evaluate cardioprotective effects of GABA-EVs^{IAT} in improving mitochondrial function and alleviating excessive oxidative stress in NMCMs during H/R. The findings suggest that in the context of H/R (Figure 2A), EVs^{IAT} has the ability to enhance the mitochondrial membrane potential of NMCMs (P = 0.0231 for H/R + EVs^{IAT} *vs* H/R group). However, it is noteworthy that GABA-EVs^{IAT} exhibits a more pronounced efficacy (Figure 2B), primarily characterized by a greater normalization of the membrane potential compared to group H/R + EVs^{IAT} (P = 0.0225 for H/R + GABA-EVs^{IAT} *vs* H/R + EVs^{IAT} group). The findings from mitochondrial OCR also align with the aforementioned conclusions (Figure 2C). In the context of H/R, EVs^{IAT} exhibit the potential to enhance both basal and maximal oxygen consumption of NMCMs mitochondria, thereby partly stabilizing aerobic respiration function in mitochondria (basal OCR: P = 0.0077 for H/R + EVs^{IAT} *vs* H/R group; maximal OCR: P = 0.0267 for H/R + EVs^{IAT} *vs* H/R group). Conversely, GABA-EVs^{IAT} demonstrate a heightened efficacy in ameliorating mitochondrial aerobic respiration function under pathological conditions induced by H/R (basal OCR: P = 0.0081 for H/R + GABA-EVs^{IAT} *vs* H/R + EVs^{IAT} group; maximal OCR: P = 0.0006 for H/R + GABA-EVs^{IAT} *vs* H/R + EVs^{IAT} group). In addition, under H/R conditions, the activation level of lysosomes in NMCMs shows a moderate decrease regulated by GABA-EVs^{IAT} (Figure 2D). This suggests that GABA-EVs^{IAT} can reduce mitochondrial damage and subsequently diminish the process of lysosomal activation for clearing damaged mitochondria (P = 0.0083 for H/R + GABA-EVs^{IAT} *vs* H/R group). The morphological assessment revealed that under H/R conditions, EVs^{IAT} and GABA-EVs^{IAT} exhibited a remarkable ability to partially fortify the intricate architecture of myocardial cell mitochondria cristae as demonstrated by transmission electron microscope assay results (Figure 2E).

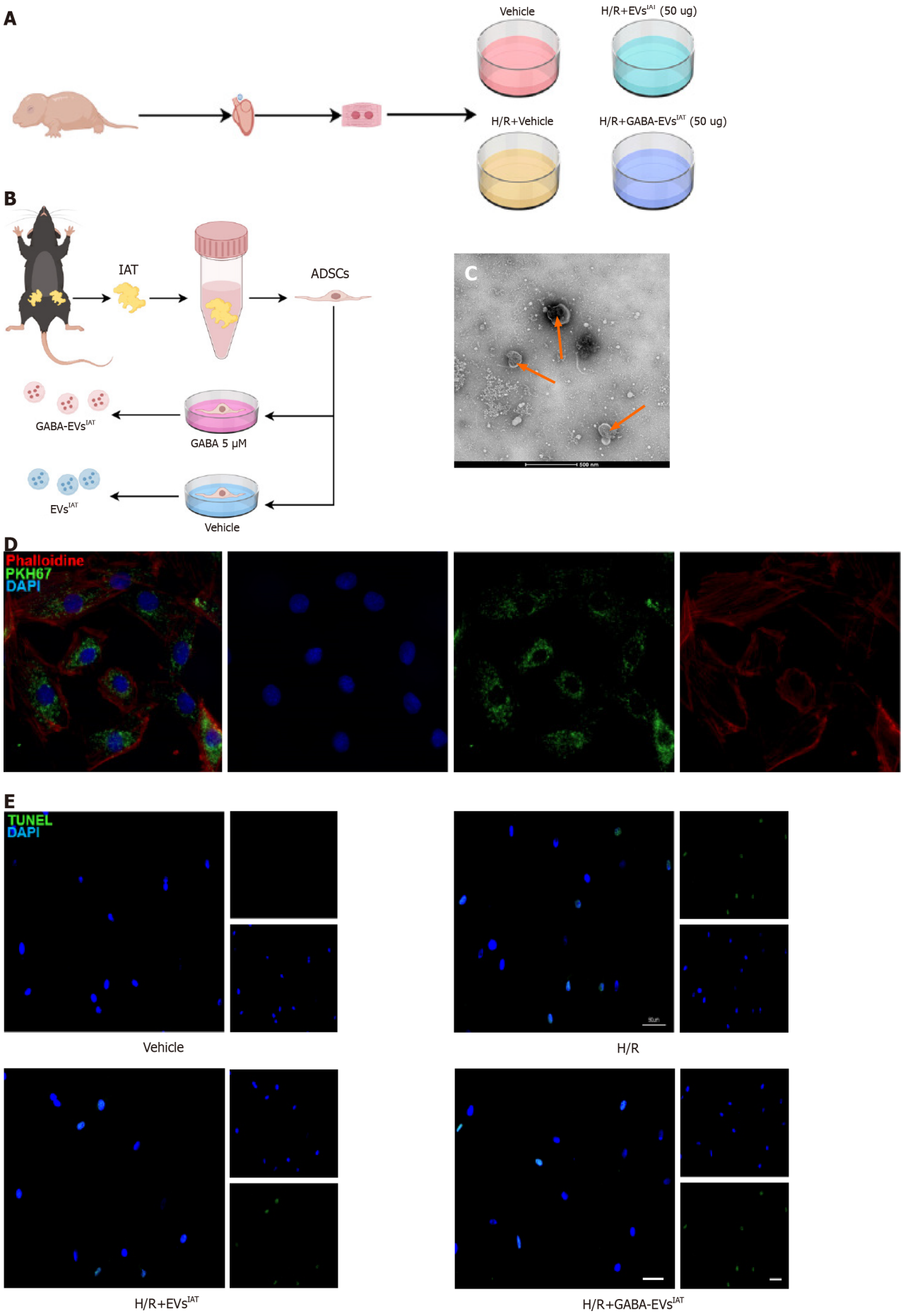
A
Vehicle
H/R+EVs^IAT (50 ug)
H/R+Vehicle
H/R+GABA-EVs^IAT (50 ug)
B
IAT
ADSCs
GABA-EVs^IAT
GABA 5 μM
EVs^IAT
Vehicle
C
D
Phalloidine
PKH67
DAPI
E
TUNEL
DAPI
Vehicle
H/R
H/R+EVs^IAT
H/R+GABA-EVs^IAT

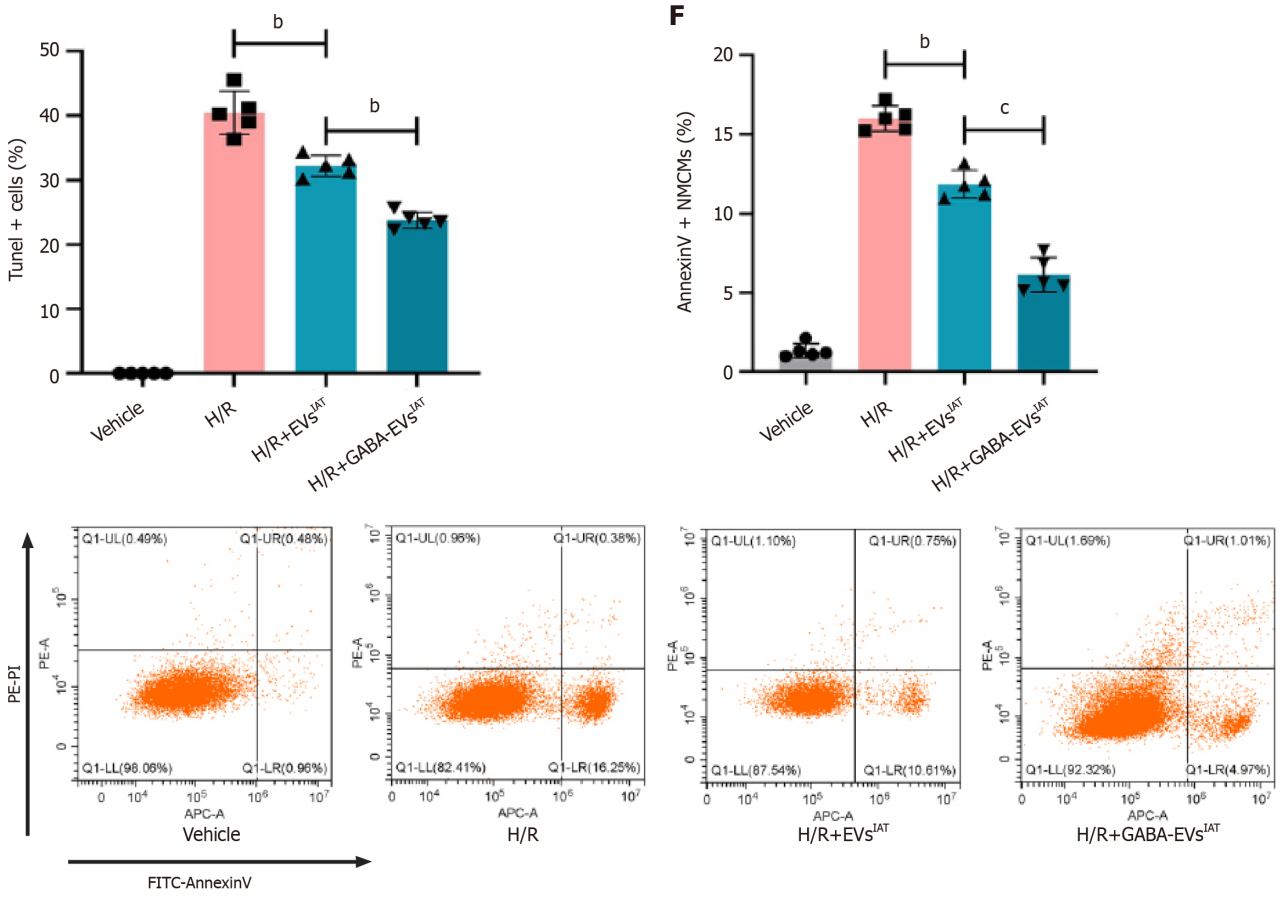

Figure 1 Gamma-aminobutyric acid-induced adipose-derived mesenchymal stem cells from inguinal adipose tissue exhibits potential in mitigating neonatal mouse cardiomyocytes injury under hypoxia and reoxygenation conditions *in vitro*. A: Experiment design. The cardiomyocytes extracted from neonatal mice were categorized into four experimental groups: Vehicle, hypoxia and reoxygenation (H/R), H/R+ extracellular vesicles (EVs) derived from adipose-derived mesenchymal stem cells (ADSCs) from inguinal adipose tissue (IAT), H/R+ gamma-aminobutyric acid (GABA)-induced ADSCs from IAT; B: Experiment design. ADSCs were extracted from the IAT of mice using an enzymatic digestion method. After incubating the ADSCs in complete medium containing 5 μM GABA for 48 h, EVs were extracted; C: Representative micrographs of EVs examined by transmission electron micrographs (scale bars = 500 nm); D: Representative micrographs of PKH67 (scale bars = 200 nm); E: Representative micrographs of isolated neonatal mouse cardiomyocytes stained with terminal deoxynucleotidyl transferase dUTP nick end-labeling (n = 5; scale bars = 200 μm); F: The percentage of AnnexinV+ neonatal mouse cardiomyocytes were calculated using flow cytometry (n = 5). $^{b}P < 0.01$, $^{c}P < 0.001$.

Administration of GABA-EVs^{IAT} mitigates myocardial damage and enhances cardiac function following MIRI

To assess the potential protective effects of GABA-EVs^{IAT} against myocardial damage induced by MIRI *in vivo*, we evaluated cardiac infarct size and AAR in mice that received in situ injections of EVs^{IAT} and GABA-EVs^{IAT} following ischemia/reperfusion (I/R) surgery. As depicted in Figure 3A, AAR/LV values were comparable among the sham, I/R, I/R + EVs^{IAT}, and I/R + GABA-EVs^{IAT} groups (re-ligating the LCA prior to Evans blue staining for AAR/LV calculation). The I/R + EVs^{IAT} and I/R + GABA-EVs^{IAT} groups exhibited significantly reduced infarct size after MIRI compared to the IR group, with the GABA-EVs^{IAT} group demonstrating the most pronounced effect (P = 0.0015 for I/R + EVs^{IAT} *vs* I/R group; P = 0.0002 for I/R + GABA-EVs^{IAT} *vs* I/R + EVs^{IAT} group). Situ apoptosis and serum cardiac markers were assessed using TUNEL assay and enzyme-linked immunosorbent assay in infarct tissues and serum samples respectively (Figure 3B). The degree of in situ apoptosis was significantly improved in both the I/R + EVs^{IAT} and I/R + GABA-EVs^{IAT} groups. I/R + GABA-EVs^{IAT} group exhibited a more remarkable reduction in apoptotic rate compared to the I/R + EVs^{IAT} group. Furthermore, the I/R + GABA-EVs^{IAT} group demonstrated a greater amelioration of serum cardiac markers than both I/R and I/R + GABA-EVs^{IAT} group. The cardiac function was assessed through animal echocardiography, revealing a remarkable enhancement in cardiac contractile function within the IR + GABA-EVs^{IAT} group when compared to both the I/R and I/R + EVs^{IAT} groups (Figure 3C).

GABA-induced miR-21-5p as a potential regulator of TXNIP in GABA-EVs^{IAT}

To explore the mechanism underlying the higher inhibitory efficacy of GABA-EVs^{IAT} on H/R-mediated cardiomyocyte injury and mitochondrial dysfunction, miRNA and mRNA sequencing was performed on EVs^{IAT} , GABA-EVs^{IAT}, and NMCMs exposed to them respectively. A total of 61 miRNAs expressed differently in GABA-EVs^{IAT} compared to EVs^{IAT} and 89 mRNA expressed differently in NMCMs exposed to EVs^{IAT} and GABA-EVs^{IAT}. The top 10 differentially expressed mRNAs and miRNAs, as identified from two sequencing results, were validated for expression using PCR (Figure 4A and B). Among those, miRNA-21-5p, miRNA-23a-3p, miRNA-199a-3p, miRNA-24-3p, miRNA-23-3p, miRNA-34-5p, and

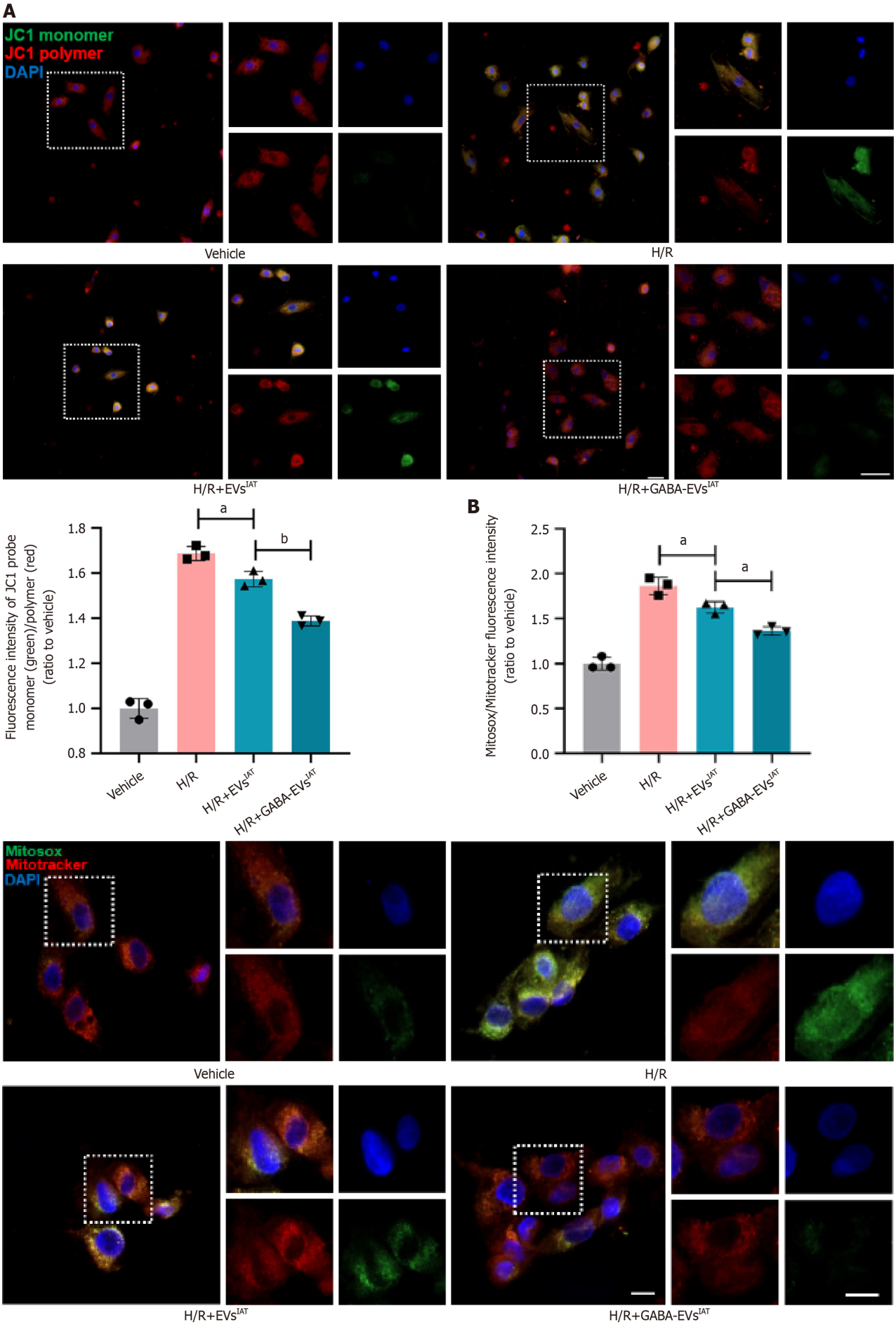
A
JC1 monomer
JC1 polymer
DAPI
Vehicle
H/R
H/R+EVs^IAT
H/R+GABA-EVs^IAT
Fluorescence intensity of JC1 probe monomer (green)/polymer (red) (ratio to vehicle)
1.8
1.6
1.4
1.2
1.0
0.8
a
b
Vehicle
H/R
H/R+EVs^IAT
H/R+GABA-EVs^IAT
B
Mitosox/Mitotracker fluorescence intensity (ratio to vehicle)
2.5
2.0
1.5
1.0
0.5
0.0
a
a
Vehicle
H/R
H/R+EVs^IAT
H/R+GABA-EVs^IAT
Mitosox
Mitotracker
DAPI
Vehicle
H/R
H/R+EVs^IAT
H/R+GABA-EVs^IAT

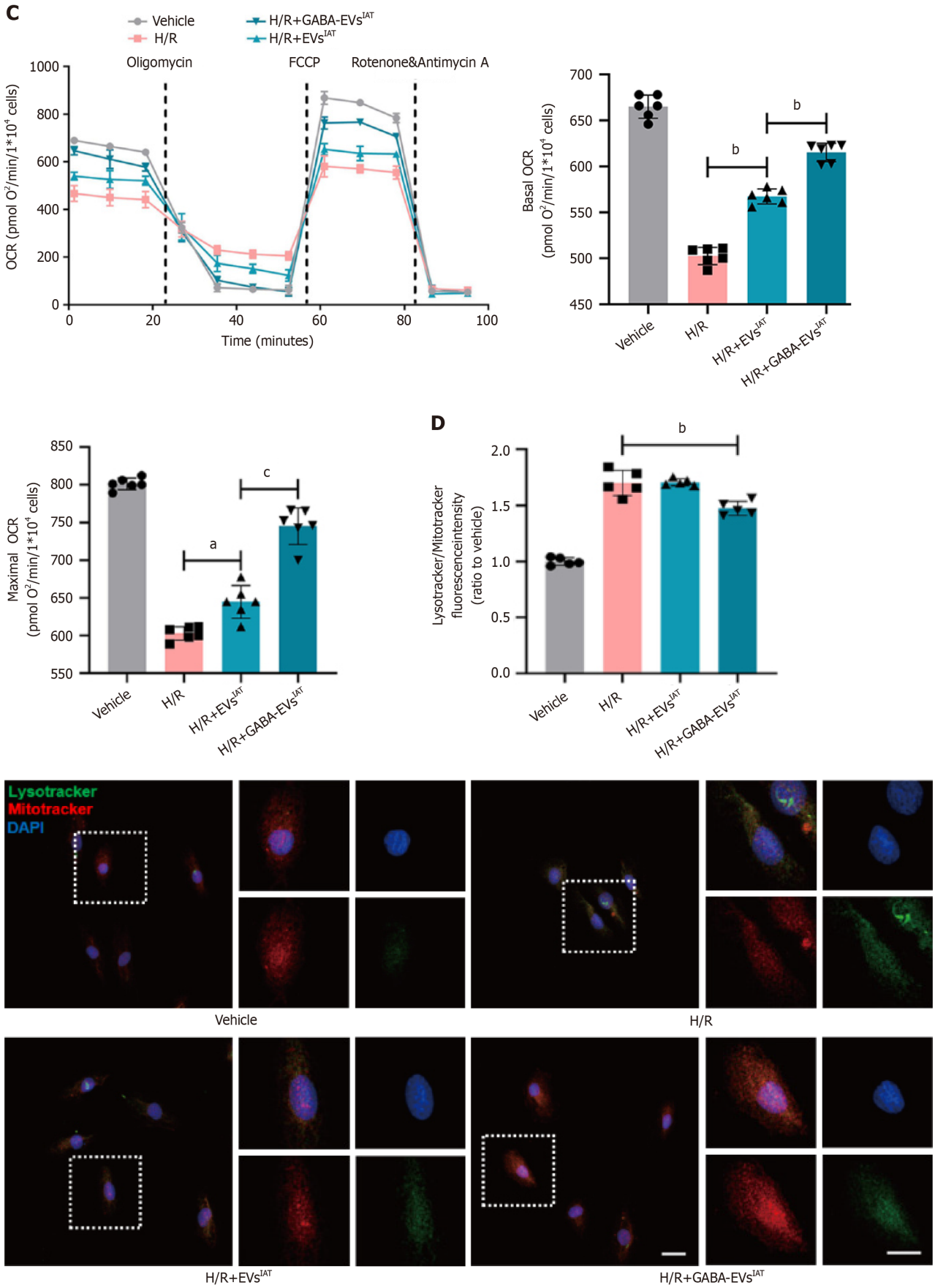
C
Vehicle
H/R
H/R+GABA-EVs^IAT
H/R+EVs^IAT
Oligomycin
FCCP
Rotenone&Antimycin A
OCR (pmol O2/min/1*10^4 cells)
Time (minutes)
Basal OCR (pmol O2/min/1*10^4 cells)
Maximal OCR (pmol O2/min/1*10^4 cells)
D
Lysotracker/Mitotracker fluorescenceintensity (ratio to vehicle)
Lysotracker
Mitotracker
DAPI
Vehicle
H/R
H/R+EVs^IAT
H/R+GABA-EVs^IAT

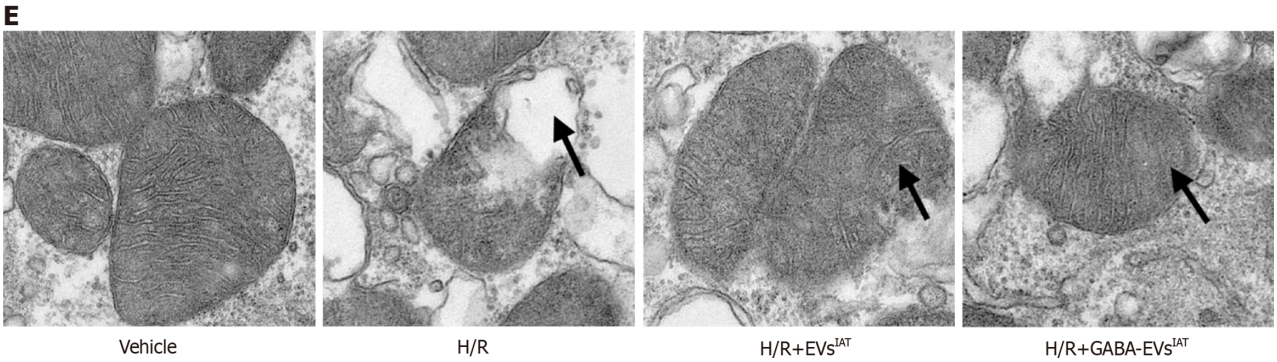

Figure 2 Gamma-aminobutyric acid-induced adipose-derived mesenchymal stem cells from inguinal adipose tissue mitigates neonatal mouse cardiomyocytes mitochondrial oxidative stress levels and enhances mitochondrial function during hypoxia and reoxygenation *in vitro*. A: Representative micrographs of isolated neonatal mouse cardiomyocytes (NMCMs) stained with JC1 probe (n = 3; scale bars = 200 μm); B: Representative micrographs of isolated NMCMs stained with mitosox probe (n = 3; scale bars = 200 μm); C: Real-time oxygen consumption rates (OCRs) and calculated basal and maximal respiration rates in NMCMs (n = 6); D: Representative micrographs of isolated NMCMs stained with mitotracker and lysotracker (n = 5; scale bars = 200 μm); E: Representative micrographs of extracellular vesicles (EVs) examined by transmission electron micrographs (scale bars = 500 nm). $^{a}P < 0.05$, $^{b}P < 0.01$, $^{c}P < 0.001$. GABA: Gamma-aminobutyric acid; H/R: Hypoxia and reoxygenation; IAT: Inguinal adipose tissue.

miRNA-214-3p were predicted to associate with TXNIP which exhibited the most pronounced decrease by the TargetScan and miRanda algorithms in the Encyclopedia of RNA Interactomes database (Figure 4C). Among the seven miRNAs predicted to bind with TXNIP, miR-21-5p was selected for further study because its upregulation was the most significant. Dual-luciferase reporter assay results showed that the fluorescence ratio was significantly reduced from HEK 293T cells upon co-transfection with miR-21-5p mimics and TXNIP wild-type-3′ UTR compared to the NC and mutant 3′ UTR controls (P = 0.0046) (Figure 4D). These results indicated that miR-21-5p inhibits the translation of TXNIP by targeting the 3′ UTR region of its mRNA.

miR-21-5p derived from GABA-EVs^{IAT} regulates TXNIP expression in NMCMs

To clarify TXNIP as the main target of EVs regulation, we assessed the protein expression of TXNIP through western blotting and immunofluorescence in NMCMs. The western blot results (Figure 5A) showed that under H/R conditions, the expression of TXNIP in NMCMs was significantly reduced in the presence of H/R + GABA-EVs^{IAT} compared to the H/R and H/R + EVs^{IAT} groups (P = 0.0008 for H/R + EVs^{IAT} *vs* H/R group; P = 0.0025 for H/R + GABA-EVs^{IAT} *vs* H/R + EVs^{IAT} group). Similarly, immunofluorescence (Figure 5B) also demonstrated the same trend in TXNIP expression (P = 0.0042 for H/R + EVs^{IAT} *vs* H/R group; P = 0.0005 for H/R + GABA-EVs^{IAT} *vs* H/R + EVs^{IAT} group). The EVs of miR-21 KO mice ADSCs were subsequently extracted following GABA induction (GABA-EVs$^{IAT\ miR\text{-}21KO}$) and schematic diagram is presented in Figure 5C. Western blotting and immunofluorescence were employed to investigate whether miR-21-5p serves as the primary regulator of TXNIP in GABA-EVs^{IAT}. After the KO of miR-21, the regulatory influence exerted by GABA-EVs$^{IAT\ miR\text{-}21KO}$ on TXNIP expression significantly diminishes (Figure 5D and E). The aforementioned research findings suggested that miR-21-5p, which is encapsulated within secretory vesicles of ADSCs^{IAT} under the influence of GABA, served as a pivotal molecule governing the expression of TXNIP in NMCMs during H/R pathological conditions.

GABA-EVs^{IAT} alleviate MIRI is by regulating NMCMs TXNIP expression through miR-21-5p incorporation

A series of rescue experiments were conducted to elucidate the causal relationship between miR-21 derived from GABA-EVs^{IAT} and its improvement on MIRI by regulating TXNIP. We generated TXNIP KO mice and isolated their NMCMs$^{TXNIP\ KO}$. The schematic diagram in this section can be referred to Figure 6A. The TUNEL detection results indicate that knocking out miR-21 in GABA-EVs^{IAT} significantly weakens the ability of GABA-EVs$^{IAT\ miR21\ KO}$ to protect NMCMs against H/R (P = 0.0006 for H/R + GABA-EVs^{IAT} *vs* H/R + GABA-EVs$^{IAT\ miR\text{-}21\ KO}$ group). However, when TXNIP in NMCMs$^{TXNIP\ KO}$ is knocked out, the above phenotype recovers (Figure 6B) (P = 0.0008 for H/R + GABA-EVs$^{IAT\ miR21\ KO}$ *vs* H/R + GABA-EVs$^{IAT\ miR21\ KO}$ + NMCMs$^{TXNIP\ KO}$ group). Simultaneously, we performed AnnexinV detection, and its findings were in concordance with the observed trend in TUNEL detection (Figure 6C) (P = 0.0005 for H/R + GABA-EVs^{IAT} *vs* H/R + GABA-EVs$^{IAT\ miR\text{-}21\ KO}$ group; P = 0.0003 for H/R + GABA-EVs$^{IAT\ miR21\ KO}$ *vs* H/R + GABA-EVs$^{IAT\ miR21\ KO}$ + NMCMs$^{TXNIP\ KO}$ group).

Subsequently, rescue experiments were conducted to investigate the phenotypic manifestation of mitochondrial function. Evaluation of mitochondrial membrane potential revealed that KO of miR-21 in GABA-EVs^{IAT} significantly attenuated the protective ability of GABA-EVs$^{IAT\ miR21\ KO}$ against H/R in NMCMs. However, this phenotype was restored when TXNIP was knocked out in NMCMs$^{TXNIP\ KO}$ (Figure 6D) (P = 0.0005 for H/R + GABA-EVs^{IAT} *vs* H/R + GABA-EVs$^{IAT\ miR\text{-}21\ KO}$ group; P = 0.0003 for H/R + GABA-EVs$^{IAT\ miR21\ KO}$ *vs* H/R + GABA-EVs$^{IAT\ miR21\ KO}$ + NMCMs$^{TXNIP\ KO}$ group). Furthermore, the oxidative decoupling function (Figure 6E) and levels of oxidative stress (Figure 6F) in NMCMs also demonstrate the aforementioned patterns (P = 0.0007 for H/R + GABA-EVs^{IAT} *vs* H/R + GABA-EVs$^{IAT\ miR\text{-}21\ KO}$ group; P = 0.0023 for H/R + GABA-EVs$^{IAT\ miR21\ KO}$ *vs* H/R + GABA-EVs$^{IAT\ miR21\ KO}$ + NMCMs$^{TXNIP\ KO}$ group). Therefore, the aforementioned findings suggested that GABA-EVs^{IAT} predominantly modulate TXNIP expression in target cells by delivering miR-21-5p, thereby conferring protection against MIRI and promoting mitochondrial homeostasis in NMCMs.

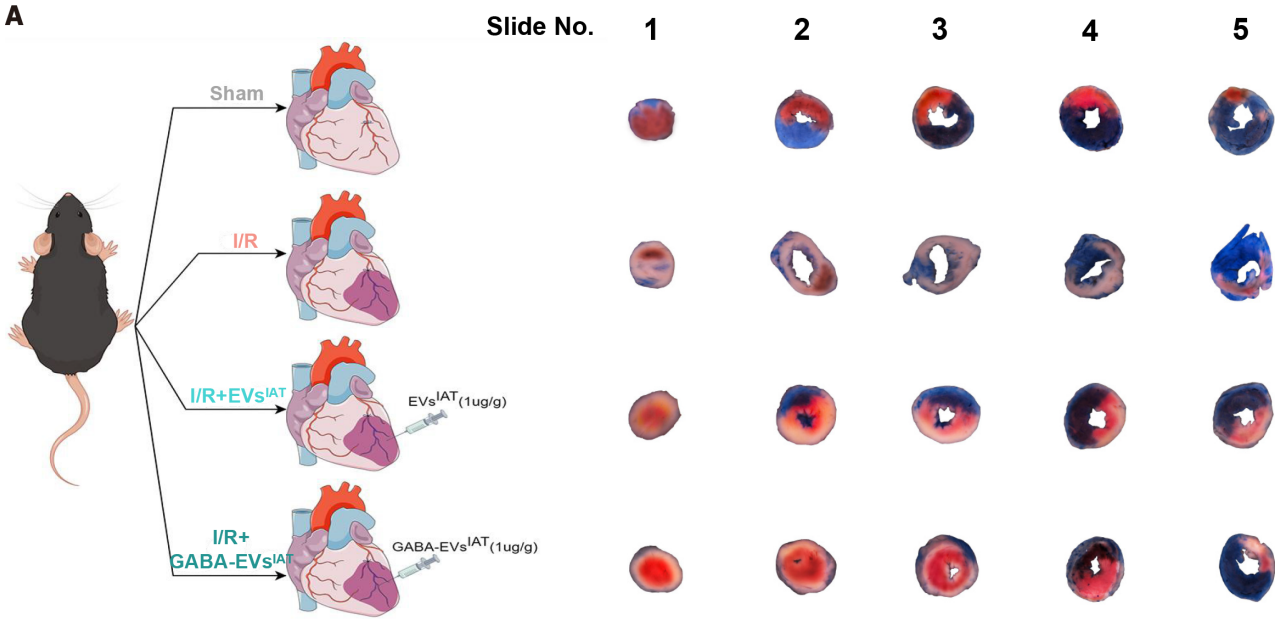
A
Slide No.
1
2
3
4
5
Sham
I/R
I/R+EVs^{IAT}
EVs^{IAT}(1ug/g)
I/R+
GABA-EVs^{IAT}
GABA-EVs^{IAT}(1ug/g)
Continuous sections of mouse heart were obtained at a thickness of 1mm/slice

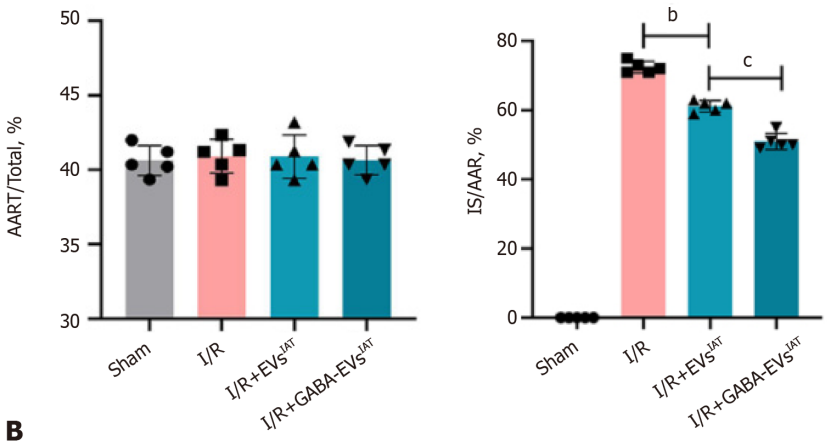
AART/Total, %
50
45
40
35
30
Sham
I/R
I/R+EVs^{IAT}
I/R+GABA-EVs^{IAT}
IS/AAR, %
80
60
40
20
0
b
c
Sham
I/R
I/R+EVs^{IAT}
I/R+GABA-EVs^{IAT}

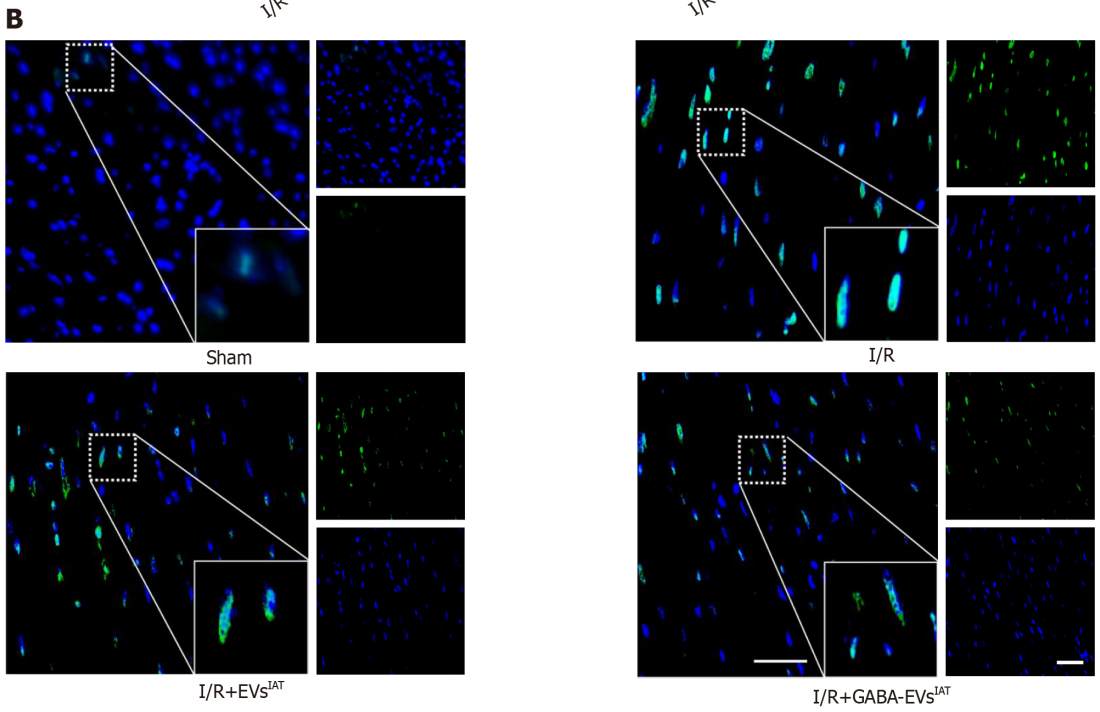
B
Sham
I/R
I/R+EVs^{IAT}
I/R+GABA-EVs^{IAT}

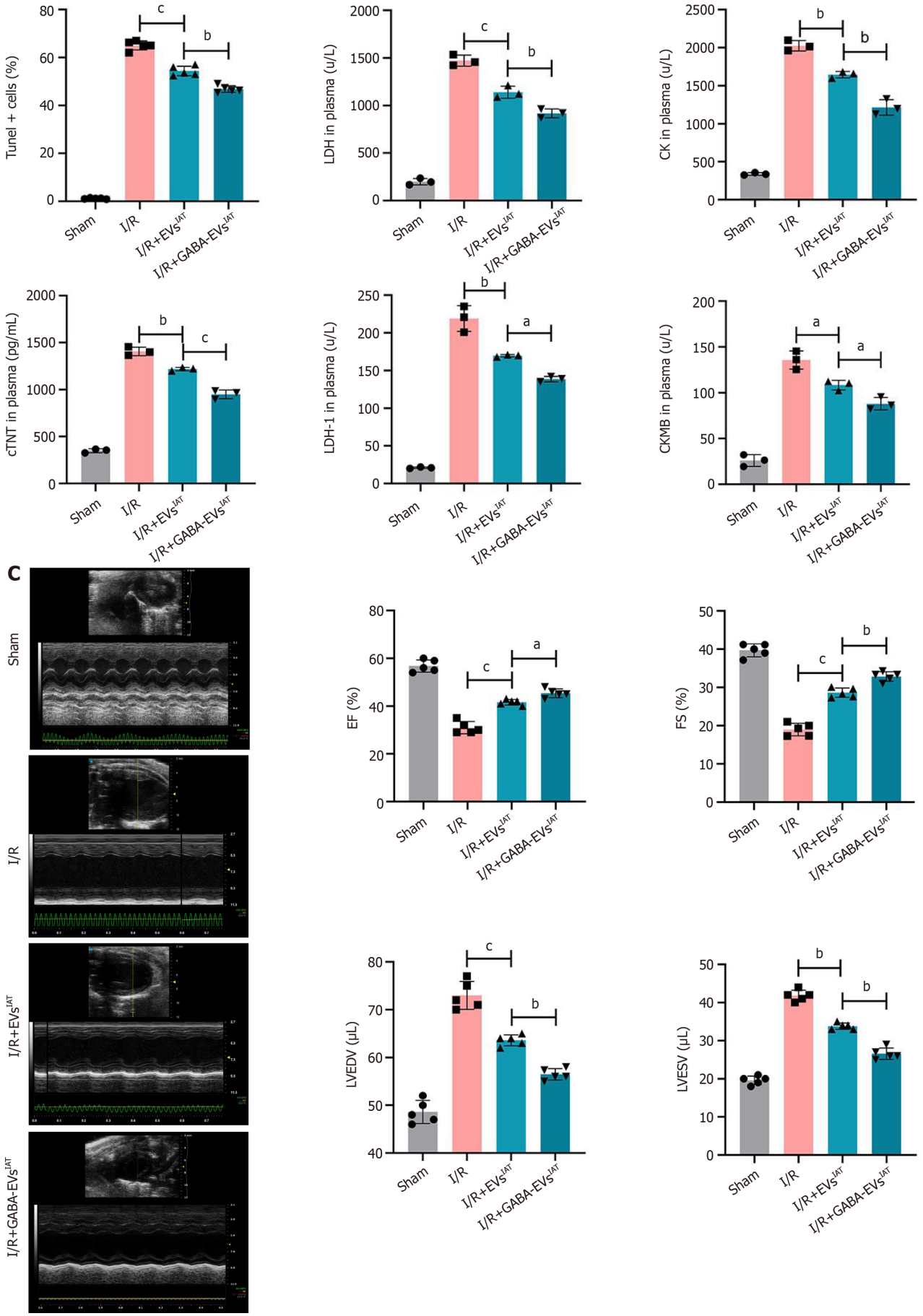

Figure 3 Gamma-aminobutyric acid-induced adipose-derived mesenchymal stem cells from inguinal adipose tissue exhibits potential in

mitigating myocardial injury and improve cardiac function under myocardial ischemia-reperfusion injury conditions *in vivo*. A: Representative graphs of Evans blue/triphenyltetrazolium chloride stain (n = 5); B: Representative micrographs of myocardial tissue section from the infarcted area stained with terminal deoxynucleotidyl transferase dUTP nick end-labeling (TUNEL) (n = 5) and serum cardiac markers degree of mice (n = 3); C: Representative M-mode images of transthoracic echocardiography, and quantification of left ventricular ejection fraction, left ventricular fraction shortening, left ventricular end diastolic volume and left ventricular end systolic volume (n = 5). $^{a}P < 0.05$, $^{b}P < 0.01$, $^{c}P < 0.001$. AAR: Area at risk; CK: Creatine kinase; cTNT: Cardiac troponin T; CKMB: Creatine kinase-MB; EF: Ejection fraction; EVs: Extracellular vesicles; FS: Fraction shortening; GABA: Gamma-aminobutyric acid; IAT: Inguinal adipose tissue; I/R: Ischemia/reperfusion; IS: Infarct size; LDH: Lactate dehydrogenase; LVEDV: Left ventricular end diastolic volume; LVESA: Left ventricular end systolic volume.

DISCUSSION

EVs are widely recognized as effective nanoscale carriers for targeted delivery of small molecules and nucleic acids to specific tissues or cells, due to their excellent biocompatibility, low immunogenicity, and ability to cross the blood-brain barrier,. Growing evidence also suggests that EVs hold great promise in delivering non-coding RNAs, cytokines, and small-molecule drugs for treating ischemic heart disease[28,29]. However, concerns remain regarding the clinical implementation of EV-based therapies[30,31]. Therefore, our objective was to enhance the therapeutic effectiveness of ADSC^{IAT}-derived EVs against MIRI through a safe GABA-induced method *in vitro* while investigating the underlying mechanisms behind the protective effects exerted by EVs.

White adipose tissue is comprised of subcutaneous fat and visceral fat. Numerous studies have substantiated that subcutaneous adipose, as opposed to visceral adipose, exerts a protective role in neighboring tissues and organs during pathological conditions. ADSCs from the IAT are regarded as one of the key cell types responsible for these effects[17]. It is noteworthy that the benefits conferred by IAT can be transferred to surrounding tissues through adipose transplantation[32]. Paracrine secretion serves as a representative regulatory pathway for these effects, with EVs being one of the most prevalent means of executing paracrine secretion[33]. It is worth noting that previous studies have confirmed the presence of GABAB receptors in ADSCs[17]. Furthermore, ADSCs derived from IAT exhibit a significantly enhanced protective effect on peripheral cells, tissues, and organs under the influence of GABA[34]. These observed disparities in biological functionality can be attributed to alterations in the qualitative and quantitative content of EVs mediated by GABA.

To explore the underlying mechanisms further, we performed multi-omics sequencing on EVs obtained from both ADSCs and cardiomyocytes. Our sequencing analysis revealed a striking discrepancy in abundance for miR-21-5p after administering GABA intervention - its levels showed a remarkable increase. However, the exact role played by miR-21 in GABA-EVs^{IAT} derived from ADSCS remains elusive at present. Consequently, we generated genetically miR-21 KO mice and isolated ADSCs from their IAT. Remarkably, our findings demonstrated that eliminating miR-21 significantly restored the effects induced by GABA treatment. It is noteworthy that the sequencing results of GABA-EVs^{IAT} *vs* EVs^{IAT} demonstrate a significant augmentation in the abundance of multiple miRNAs within the GABA-EVs^{IAT}. However, upon KO of miR-21, the antagonistic impact of GABA-EVs^{IAT} on MIRI and NMCM protection is substantially impeded. This phenotypic alteration suggests that miR-21 serves as a pivotal regulatory miRNA molecule within GABA-EVs^{IAT} for modulating myocardial protective effects under pathological conditions associated with MIRI.

Additionally, transcriptome sequencing was performed on recipient myocardial cells of EVs. As anticipated, the expression of TXNIP exhibited a significant reduction in the GABA-induced EVs intervention group. Dual luciferase reporter gene assays and rescue experiments further validated that TXNIP is among the target genes regulated by miR-21-5p. The induction of ADSCs by GABA leads to a heightened abundance of miR-21 within EVs, thereby suppressing the expression of TXNIP in target cells. This represents one of the fundamental mechanisms through which GABA exerts its protective efficacy in MIRI.

Previous evidence indicates that TXNIP is responsible for coordinating a multitude of cellular responses, including stress, inflammation, and programmed cell death[35,36]. As an inaugural stride in MIRI, the regulation of mitochondrial oxidative stress is deftly governed by TXNIP[37]. As a key reducing molecule that counteracts oxidative stress within mitochondria and as one of the target molecules for TXNIP-induced oxidative stress, TRX2 is known to bind with (apoptosis signal-regulating kinase 1) under stable conditions, thereby inhibiting apoptosis signal-regulating kinase 1-mediated phosphorylation regulation downstream and activating mechanisms such as apoptosis, inflammation, and ferroptosis[38]. This molecular-level change is mainly attributed to the binding and degradation of *TXNIP* mRNA by miR-21-5p derived from EVs, which subsequently alleviates the association between TXNIP and TRX2, rescuing excessive oxidative stress.

In our previous study, we have unveiled EVs derived from ADSCs primarily targeting TXNIP to alleviate myocardial ischemia reperfusion injury[39]. Theoretically and mechanically, TXNIP, interacting with hypoxia-inducible factor-1 alpha, involves the degradation of hypoxia-inducible factor-1 alpha and induces pyroptosis. Thus, by targeting TXNIP, GABA-EVs^{IAT} effectively improve the prognosis of MIRI by means of various intricate mechanisms. It should be duly noted that EVs derived from different sources of ADSCs exhibit distinct biological effects. Presently, it is widely acknowledged that EVs originating from ADSCs^{IAT} possess the remarkable capability to ameliorate pathological conditions such as inflammation, oxidative stress, and insulin resistance[40,41]. Conversely, EVs obtained from ADSCs derived from visceral adipose tissue lack these aforementioned effects[42]. Henceforth, in this study, we procured subcutaneous adipose tissue from the inguinal region in accordance with prior experimental findings.

From a clinical perspective, if the duration of MI surpasses the therapeutic time window of approximately 12 h, during which cardiomyocytes undergo irreversible cell death, even reperfusion therapy proves futile[43,44]. It is postulated that timely initiation of reperfusion therapy is paramount; therefore, interventions aimed at bolstering cardiomyocyte survival

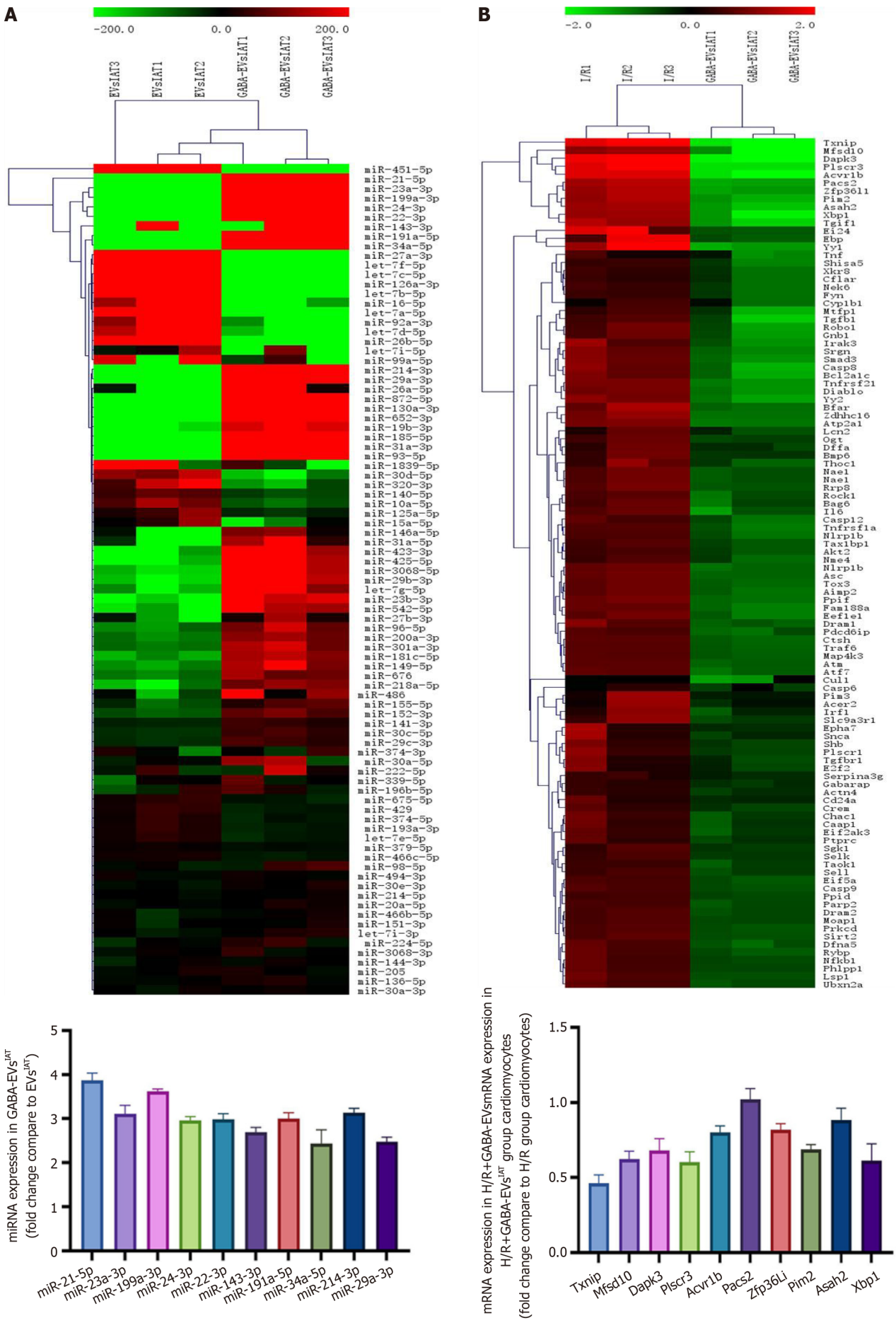
A
-200.0
0.0
200.0
EVsIAT3
EVsIAT1
EVsIAT2
GABA-EVsIAT1
GABA-EVsIAT2
GABA-EVsIAT3
miR-451-5p
miR-21-5p
miR-23a-3p
miR-199a-3p
miR-24-3p
miR-22-3p
miR-143-3p
miR-191a-5p
miR-34a-5p
miR-27a-3p
let-7f-5p
let-7c-5p
miR-126a-3p
let-7b-5p
miR-16-5p
let-7a-5p
miR-92a-3p
let-7d-5p
miR-26b-5p
let-7i-5p
miR-99a-5p
miR-214-3p
miR-29a-3p
miR-26a-5p
miR-872-5p
miR-130a-3p
miR-652-3p
miR-19b-3p
miR-185-5p
miR-31a-3p
miR-93-5p
miR-1839-5p
miR-30d-5p
miR-320-3p
miR-140-5p
miR-10a-5p
miR-125a-5p
miR-15a-5p
miR-146a-5p
miR-31a-5p
miR-423-3p
miR-425-5p
miR-3068-5p
miR-29b-3p
let-7g-5p
miR-23b-3p
miR-542-5p
miR-27b-3p
miR-96-5p
miR-200a-3p
miR-301a-3p
miR-181c-5p
miR-149-5p
miR-676
miR-218a-5p
miR-486
miR-155-5p
miR-152-3p
miR-141-3p
miR-30c-5p
miR-29c-3p
miR-374-3p
miR-30a-5p
miR-222-5p
miR-339-5p
miR-196b-5p
miR-675-5p
miR-429
miR-374-5p
miR-193a-3p
let-7e-5p
miR-379-5p
miR-466c-5p
miR-98-5p
miR-494-3p
miR-30e-3p
miR-214-5p
miR-20a-5p
miR-466b-5p
miR-151-3p
let-7i-3p
miR-224-5p
miR-3068-3p
miR-144-3p
miR-205
miR-136-5p
miR-30a-3p
B
-2.0
0.0
2.0
I/R1
I/R2
I/R3
GABA-EVsIAT1
GABA-EVsIAT2
GABA-EVsIAT3
Txnip
Mfsd10
Dapk3
Plscr3
Acvr1b
Pacs2
Zfp36l1
Pim2
Asah2
Xbp1
Tgif1
Ei24
Ebp
Yy1
Tnf
Shisa5
Xkr8
Cflar
Nek6
Fyn
Cyp1b1
Mtfp1
Tgfb1
Robo1
Gnb1
Irak3
Srgn
Smad3
Casp8
Bcl2a1c
Tnfrsf21
Diablo
Yy2
Bfar
Zdhhc16
Atp2a1
Lcn2
Ogt
Dffa
Bmp6
Thoc1
Nae1
Nae1
Rrp8
Rock1
Bag6
Il6
Casp12
Tnfrsf1a
Nlrp1b
Tax1bp1
Akt2
Nme4
Nlrp1b
Asc
Tox3
Aimp2
Ppif
Fam188a
Eef1e1
Dram1
Pdcd6ip
Ctsh
Traf6
Map4k3
Atm
Atf7
Cul1
Casp6
Pim3
Acer2
Irf1
Slc9a3r1
Epha7
Snca
Shb
Plscr1
Tgfbr1
E2f2
Serpina3g
Gabarap
Actn4
Cd24a
Crem
Chac1
Caap1
Eif2ak3
Ptprc
Sgk1
Selk
Taok1
Sell
Eif5a
Casp9
Ppid
Parp2
Dram2
Moap1
Prkcd
Sirt2
Dfna5
Rybp
Nfkb1
Phlpp1
Lsp1
Ubxn2a
miRNA expression in GABA-EVs^{IAT} (fold change compare to EVs^{IAT})
5
4
3
2
1
0
miR-21-5p
miR-23a-3p
miR-199a-3p
miR-24-3p
miR-22-3p
miR-143-3p
miR-191a-5p
miR-34a-5p
miR-214-3p
miR-29a-3p
mRNA expression in H/R+GABA-EVsmRNA expression in H/R+GABA-EVs^{IAT} group cardiomyocytes (fold change compare to H/R group cardiomyocytes)
1.5
1.0
0.5
0.0
Txnip
Mfsd10
Dapk3
Plscr3
Acvr1b
Pacs2
Zfp36Li
Pim2
Asah2
Xbp1

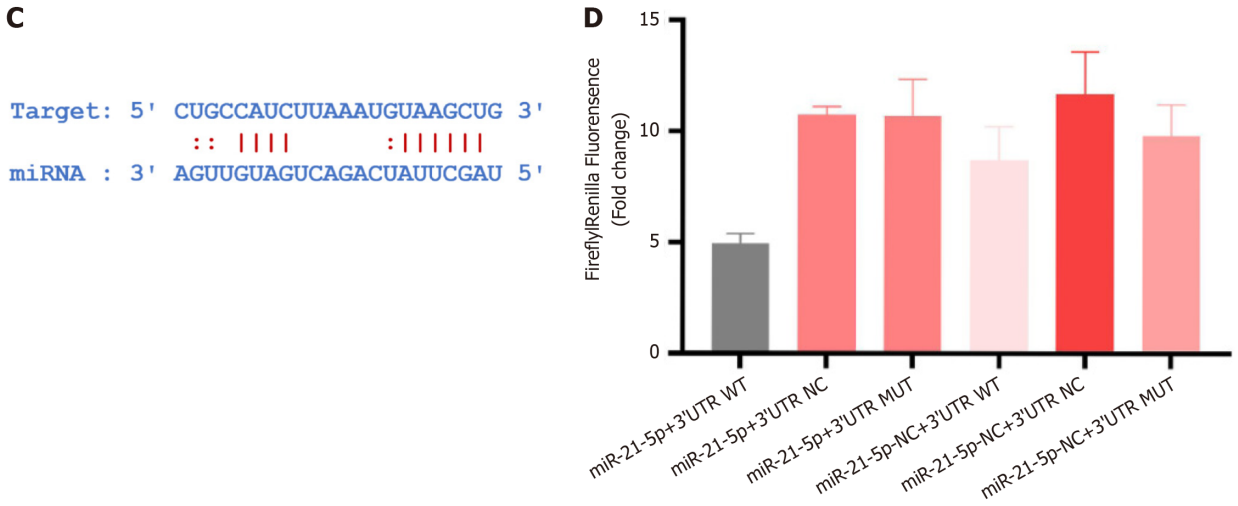

Figure 4 MicroRNA-21-5p derived from gamma-aminobutyric acid-induced adipose-derived mesenchymal stem cells from inguinal adipose tissue regulate thioredoxin-interacting protein expression in mRNA degree. A: MicroRNA (miRNA) sequencing results of gamma-aminobutyric acid (GABA)-induced adipose-derived mesenchymal stem cells (ADSCs) from inguinal adipose tissue (IAT) *vs* extracellular vesicles (EVs)^{IAT}; B: mRNA sequencing results of neonatal mouse cardiomyocytes exposed to GABA-induced ADSCs from IAT; C: Binding sites predicted for the 3' untranslated region (UTR) regions of thioredoxin-interacting protein and miR-21-5p; D: Validation of the binding between thioredoxin-interacting protein and miR-21-5p using a dual luciferase reporter gene assay. H/R: Hypoxia and reoxygenation; miRNA: MicroRNA; MUT: Mutated; NC: Negative control; WT: Wild-type.

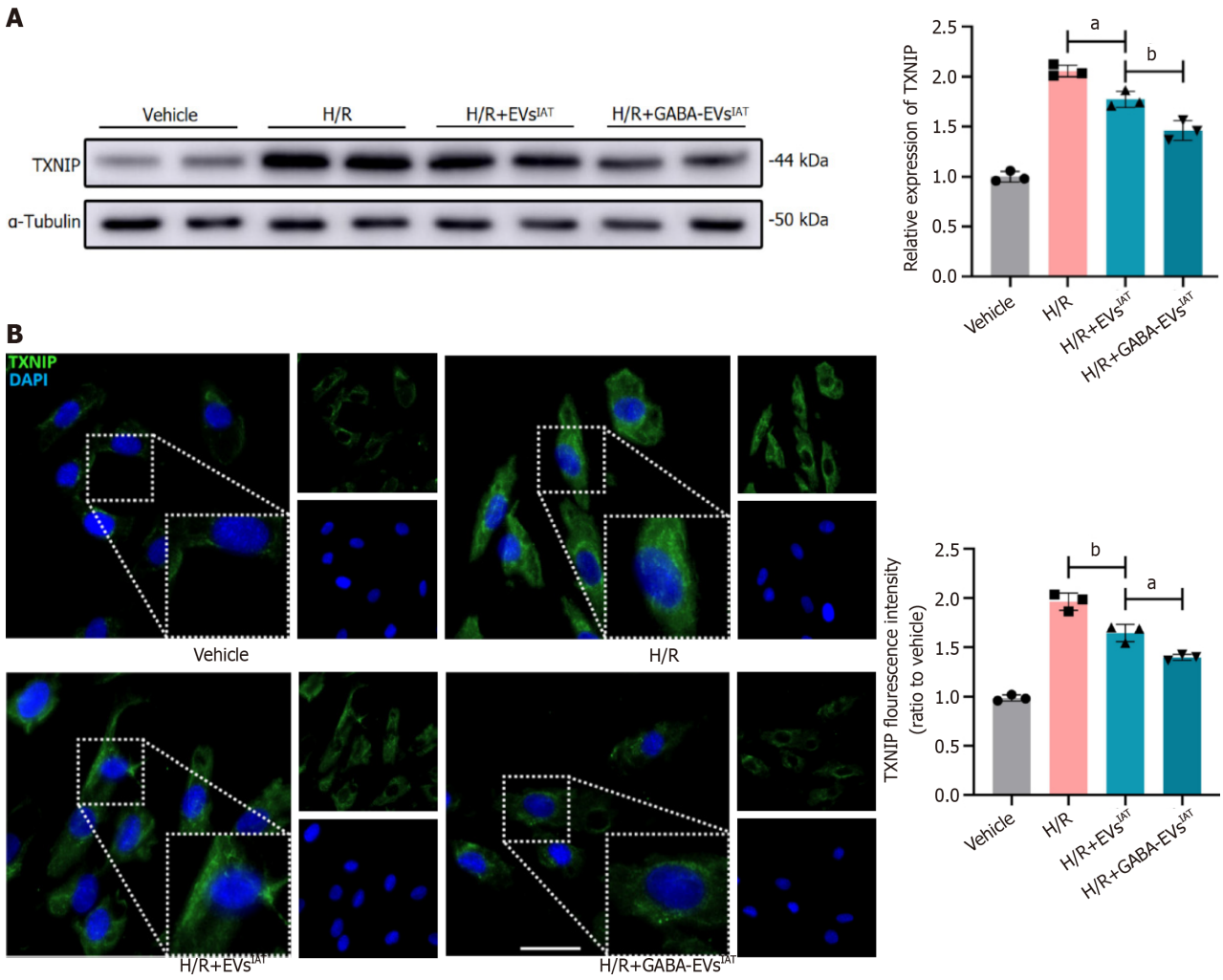

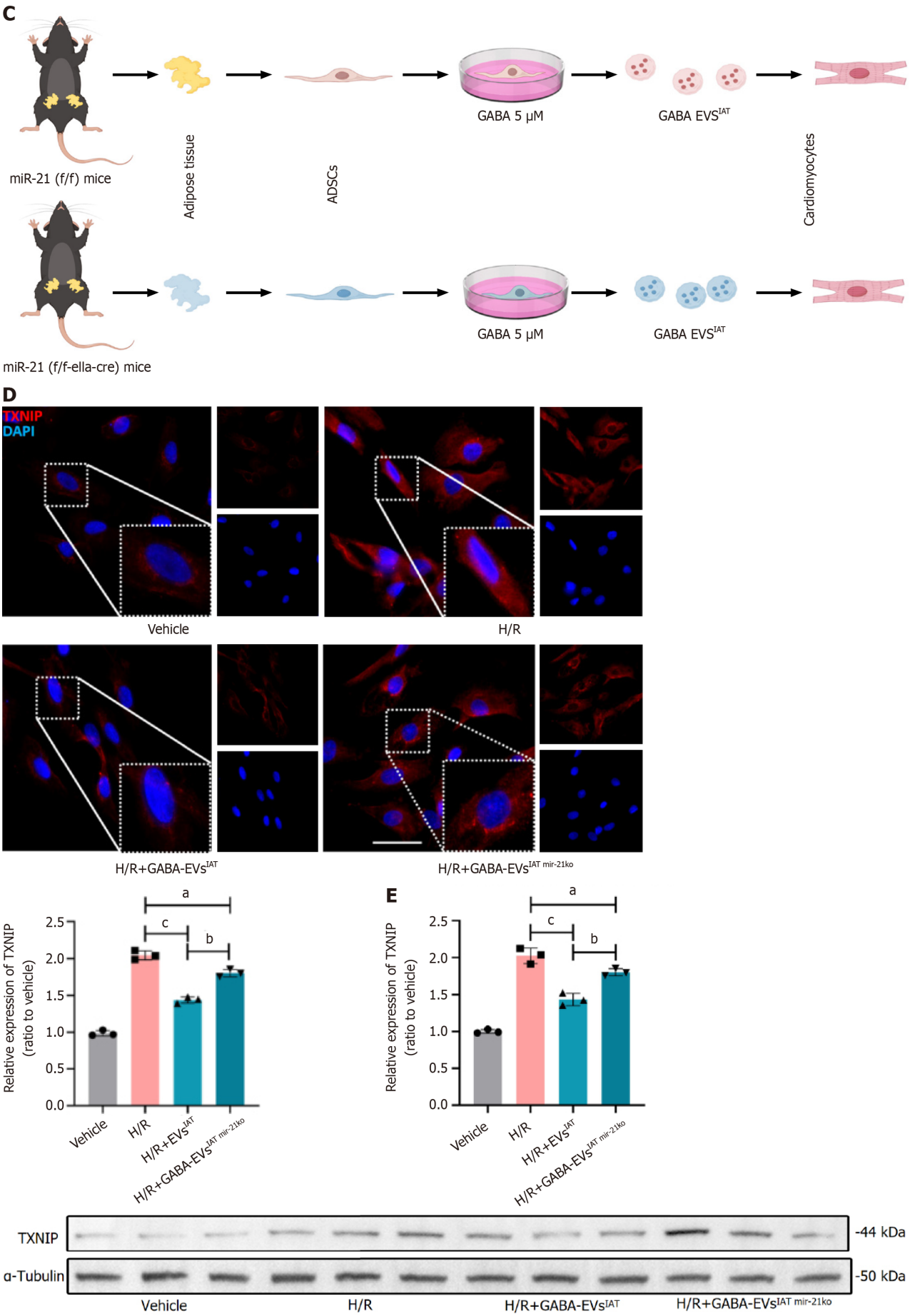

Figure 5 MicroR-21-5p derived from gamma-aminobutyric acid-induced adipose-derived mesenchymal stem cells from inguinal adipose

tissue regulate thioredoxin-interacting protein expression in protein degree. A: Representative immunoblots and quantitative analysis of thioredoxin-interacting protein (TXNIP) at the protein level in neonatal mouse cardiomyocytes (NMCMs) (n = 3); B: Representative micrographs of NMCMs stained with TXNIP antibody (n = 3; scale bars = 200 μm); C: Experiment design. Adipose-derived mesenchymal stem cells (ADSCs) were isolated from both miR-21 KO and miR-21$^{f/f}$ mice inguinal adipose tissue (IAT), and extracellular vesicles (EVs) were extracted respectively; D: Representative micrographs of NMCMs stained with TXNIP antibody (n = 3; scale bars = 200 μm); E: Representative immunoblots and quantitative analysis of TXNIP at the protein level in NMCMs (n = 3). $^{a}P < 0.05$, $^{b}P < 0.01$, $^{c}P < 0.001$. GABA: Gamma-aminobutyric acid; H/R: Hypoxia and reoxygenation.

from the onset of MI until reperfusion therapy become particularly significant. It is assumed that reperfusion therapy can be performed in a fixed time period, then therapies that support cardiomyocytes to survive from onset of MI to reperfusion therapy are particularly significant. Hence, the implementation of early reperfusion strategies for occluded blood vessels and proactive intervention in MIRI are two pivotal treatment approaches aimed at safeguarding a greater number of myocardial cells from succumbing to catastrophic damage following a cardiac event. In conclusion, our study demonstrates that GABA-EVs^{IAT} show a more significant cardioprotection against MIRI than EVs^{IAT}, which partly is attributed to the abundant load of miR-21-5p targeting TXNIP, thereby exacerbating cardiomyocyte mitochondrial oxidative stress levels and facilitating the progression of programmed cell death in cardiomyocytes.

CONCLUSION

In conclusion, our study demonstrated that EVs derived from ADSCs obtained from IAT treated with GABA exhibited significant cardioprotective effects against mitochondrial oxidative stress. These protective effects may be attributed to the ability of EVs to deliver miR-21-5p, which targets TXNIP, thereby regulating the formation of TXNIP-TRX complexes and subsequently enhancing TRX's antioxidant activity (Figure 7 graphical abstract).

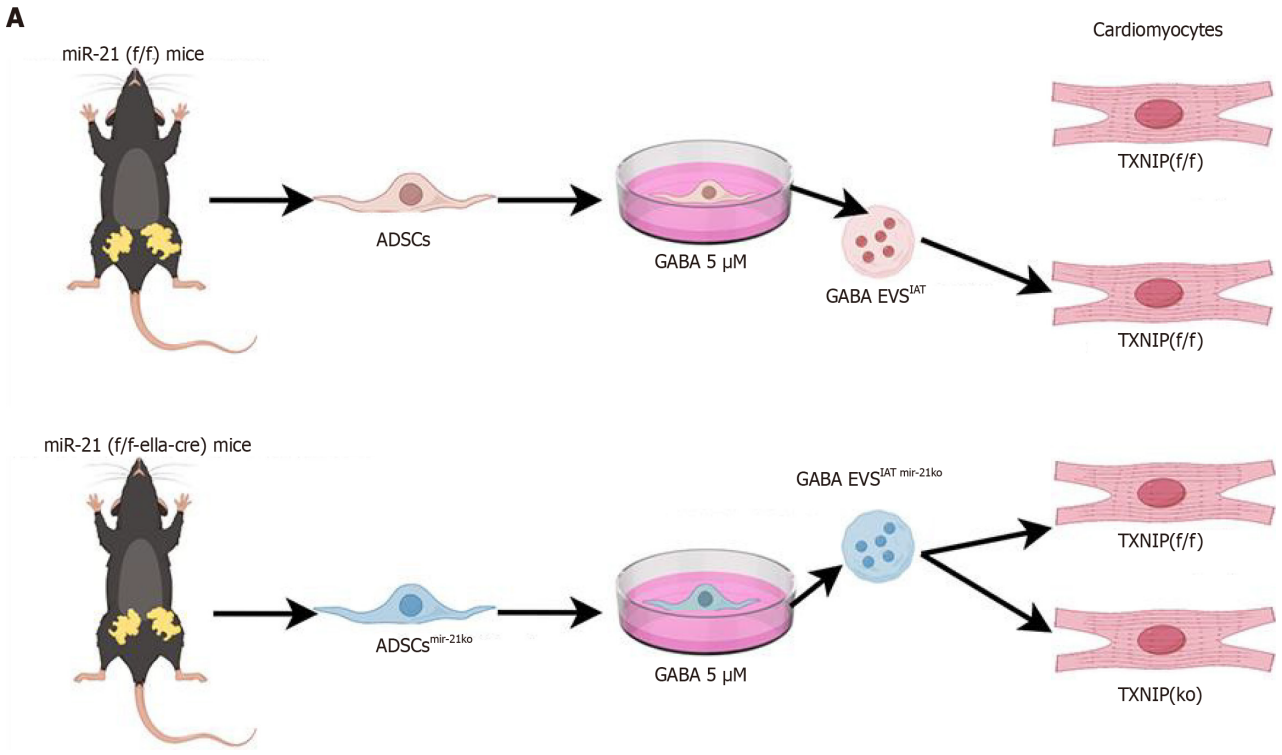

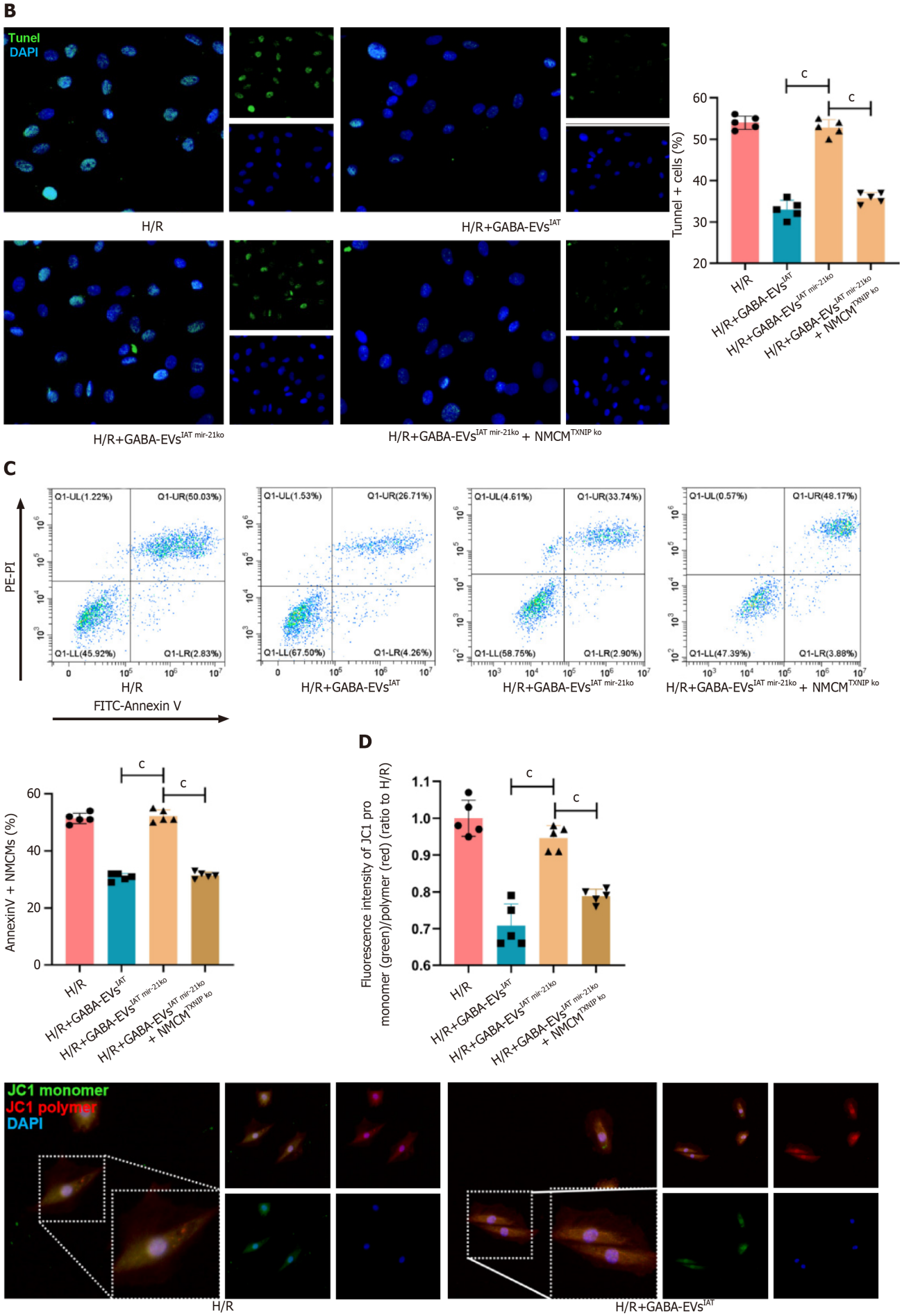
B
Tunel
DAPI
H/R
H/R+GABA-EVs^IAT
H/R+GABA-EVs^IAT mir-21ko
H/R+GABA-EVs^IAT mir-21ko + NMCM^TXNIP ko
Tunnel + cells (%)
C
C
H/R
H/R+GABA-EVs^IAT
H/R+GABA-EVs^IAT mir-21ko
H/R+GABA-EVs^IAT mir-21ko + NMCM^TXNIP ko
C
PE-PI
FITC-Annexin V
Q1-UL(1.22%)
Q1-UR(50.03%)
Q1-LL(45.92%)
Q1-LR(2.83%)
Q1-UL(1.53%)
Q1-UR(26.71%)
Q1-LL(67.50%)
Q1-LR(4.26%)
Q1-UL(4.61%)
Q1-UR(33.74%)
Q1-LL(58.75%)
Q1-LR(2.90%)
Q1-UL(0.57%)
Q1-UR(48.17%)
Q1-LL(47.39%)
Q1-LR(3.88%)
H/R
H/R+GABA-EVs^IAT
H/R+GABA-EVs^IAT mir-21ko
H/R+GABA-EVs^IAT mir-21ko + NMCM^TXNIP ko
AnnexinV + NMCMs (%)
C
C
H/R
H/R+GABA-EVs^IAT
H/R+GABA-EVs^IAT mir-21ko
H/R+GABA-EVs^IAT mir-21ko + NMCM^TXNIP ko
D
Fluorescence intensity of JC1 pro monomer (green)/polymer (red) (ratio to H/R)
C
C
H/R
H/R+GABA-EVs^IAT
H/R+GABA-EVs^IAT mir-21ko
H/R+GABA-EVs^IAT mir-21ko + NMCM^TXNIP ko
JC1 monomer
JC1 polymer
DAPI
H/R
H/R+GABA-EVs^IAT

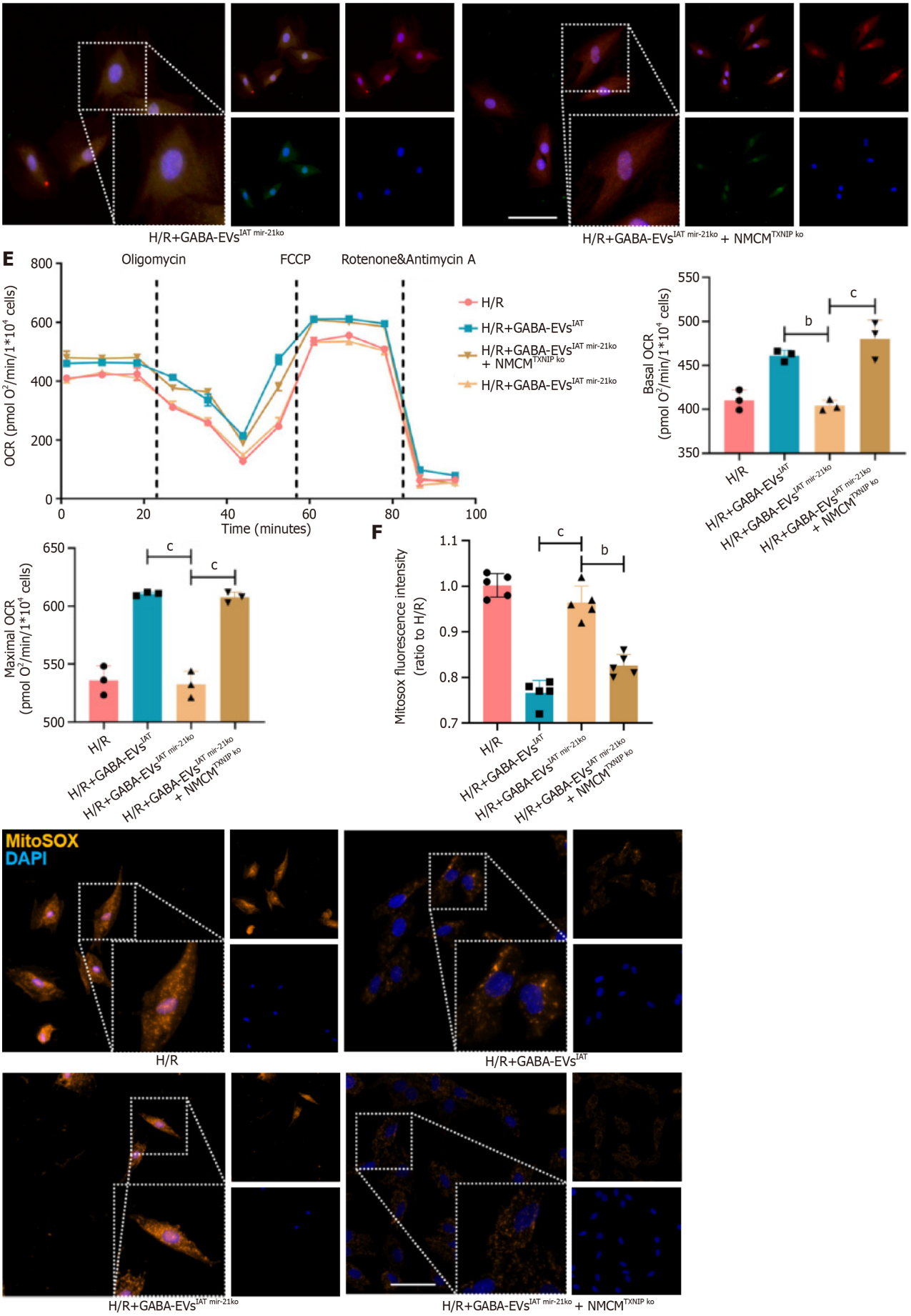

Figure 6 Extracellular vesicles derived from adipose-derived mesenchymal stem cells from inguinal adipose tissue-associated microRNA-

21-5p alleviates hypoxia and reoxygenation-mediated myocardial injury and mitochondrial dysfunctions by downregulating thioredoxin-interacting protein. A: Experiment design. Adipose-derived mesenchymal stem cells (ADSCs) were isolated from both microRNA-21 (miR-21) knockout (KO) and miR-21$^{f/f}$ mouse inguinal adipose tissue (IAT), and extracellular vesicles (EVs) were extracted respectively. Neonatal mouse cardiomyocytes (NMCMs) and NMCMs$^{TXNIP\ KO}$ were respectively treated with gamma-aminobutyric acid (GABA)-induced ADSCs from IAT (GABA-EVs^{IAT}) and GABA-EVs$^{IAT\ miR\ 21KO}$; B: Representative micrographs of NMCMs stained with thioredoxin-interacting protein (TXNIP) antibody (n = 5; scale bars = 200 μm); C: The percentage of AnnexinV+ NMCMs was calculated using flow cytometry (n = 5); D: Representative micrographs of isolated NMCMs stained with JC1 probe (n = 5; scale bars = 200 μm); E: Real-time oxygen consumption rates (OCRs) and calculated basal and maximal respiration rates in NMCMs (n = 3); F: Representative micrographs of isolated NMCMs stained with mitosox probe (n = 5; scale bars = 200 μm). $^{b}P < 0.01$, $^{c}P < 0.001$, $^{d}P < 0.0001$. H/R: Hypoxia and reoxygenation; TUNEL: Terminal deoxynucleotidyl transferase dUTP nick end-labeling.

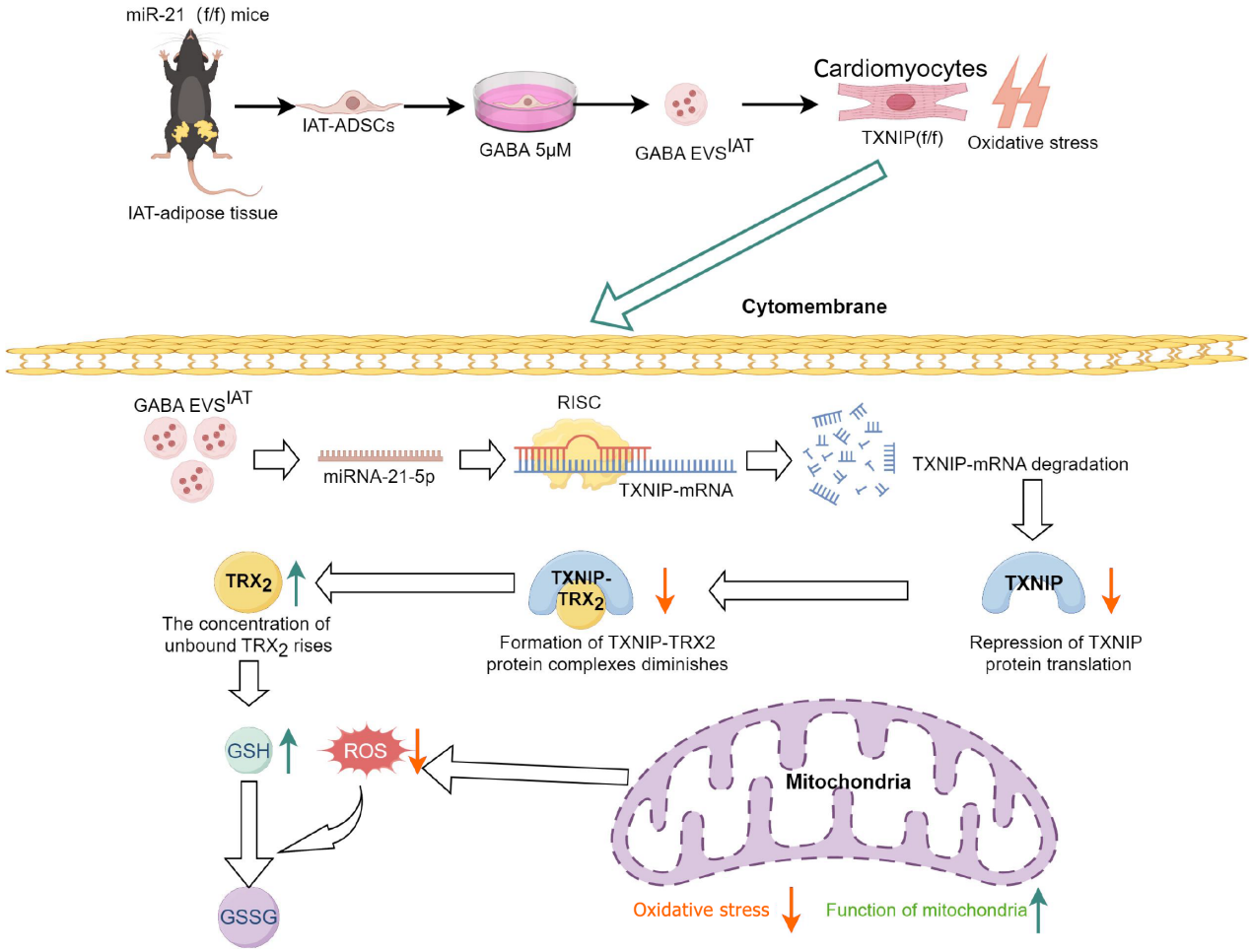

Figure 7 Graphical abstract. Adipose-derived mesenchymal stem cells (ADSCs) derived from subcutaneous adipose tissue, under the influence of gamma-aminobutyric acid (GABA), secrete extracellular vesicles (EVs) abundant in microRNA-21-5p. These EVs possess the ability to impede intracellular thioredoxin-interacting protein (TXNIP) expression in cardiomyocytes, thereby modulating the formation of TXNIP-thioredoxin 2 complex and facilitating thioredoxin 2 involvement in regulating mitochondrial oxidative stress. Consequently, this diminishes the level of mitochondrial oxidative stress in cardiomyocytes and confers protective effects on cardiomyocytes under pathological conditions such as myocardial ischemia-reperfusion injury. GSH: Glutathione; IAT: Inguinal adipose tissue; ROS: Reactive oxygen species; TRX2: Thioredoxin 2.

FOOTNOTES

Author contributions: Wang FD, Ding Y, and Zhou JH contributed equally to this work in performance of the experiments, and review and editing of the manuscript; Zhou E, Zhang TT, Fan YQ, He Q, and Zhang ZQ wrote the paper; Mao CY provided funding for this study; Mao CY, Zhang JF, and Zhou J conceived the study and contributed equally to this work. Wang FD and Ding Y are the co-first authors of this manuscript. Mao CY and Zhou J are the co-corresponding authors of this manuscript. All authors read and approved the final manuscript.

Supported by the National Natural Science Foundation of China, No. 82200270.

Institutional animal care and use committee statement: All animal procedures were approved by the Shanghai Ninth People's Hospital Institutional Ethics Committee (Approval No. SH9H-2022-A517-SB) and conducted in accordance with the guidelines of the Directive 2010/63/EU of the European Parliament.

Conflict-of-interest statement: The authors have no conflicts of interest to declare.

Data sharing statement: The data that support the findings of this study are available from the corresponding author upon reasonable request.

ARRIVE guidelines statement: The authors have read the ARRIVE guidelines, and the manuscript was prepared and revised according to the ARRIVE guidelines.

Country of origin: China

ORCID number: En Zhou 0000-0002-6073-8037; Tian-Tian Zhang 0000-0001-8218-2757; Yu-Qi Fan 0000-0002-0084-2895; Qing He 0000-0002-1078-350X; Cheng-Yu Mao 0000-0001-9740-8835; Jun-Feng Zhang 0000-0001-9530-3263; Jing Zhou 0009-0004-4740-7884.

S-Editor: Wang JJ
L-Editor: Filipodia
P-Editor: Guo X

REFERENCES

1 **Vogel B**, Claessen BE, Arnold SV, Chan D, Cohen DJ, Giannitsis E, Gibson CM, Goto S, Katus HA, Kerneis M, Kimura T, Kunadian V, Pinto DS, Shiomi H, Spertus JA, Steg PG, Mehran R. ST-segment elevation myocardial infarction. *Nat Rev Dis Primers* 2019; **5**: 39 [PMID: 31171787 DOI: 10.1038/s41572-019-0090-3]

2 **Hayes SN**, Tweet MS, Adlam D, Kim ESH, Gulati R, Price JE, Rose CH. Spontaneous Coronary Artery Dissection: JACC State-of-the-Art Review. *J Am Coll Cardiol* 2020; **76**: 961-984 [PMID: 32819471 DOI: 10.1016/j.jacc.2020.05.084]

3 **Frangogiannis NG**. Pathophysiology of Myocardial Infarction. *Compr Physiol* 2015; **5**: 1841-1875 [PMID: 26426469 DOI: 10.1002/cphy.c150006]

4 **James TN**. The variable morphological coexistence of apoptosis and necrosis in human myocardial infarction: significance for understanding its pathogenesis, clinical course, diagnosis and prognosis. *Coron Artery Dis* 1998; **9**: 291-307 [PMID: 9710689 DOI: 10.1097/00019501-199809050-00007]

5 **Sato T**, Machida T, Takahashi S, Iyama S, Sato Y, Kuribayashi K, Takada K, Oku T, Kawano Y, Okamoto T, Takimoto R, Matsunaga T, Takayama T, Takahashi M, Kato J, Niitsu Y. Fas-mediated apoptosome formation is dependent on reactive oxygen species derived from mitochondrial permeability transition in Jurkat cells. *J Immunol* 2004; **173**: 285-296 [PMID: 15210786 DOI: 10.4049/jimmunol.173.1.285]

6 **Burke AP**, Virmani R. Pathophysiology of acute myocardial infarction. *Med Clin North Am* 2007; **91**: 553-72; ix [PMID: 17640536 DOI: 10.1016/j.mcna.2007.03.005]

7 **Zhou R**, Tardivel A, Thorens B, Choi I, Tschopp J. Thioredoxin-interacting protein links oxidative stress to inflammasome activation. *Nat Immunol* 2010; **11**: 136-140 [PMID: 20023662 DOI: 10.1038/ni.1831]

8 **Shin D**, Jeon JH, Jeong M, Suh HW, Kim S, Kim HC, Moon OS, Kim YS, Chung JW, Yoon SR, Kim WH, Choi I. VDUP1 mediates nuclear export of HIF1alpha *via* CRM1-dependent pathway. *Biochim Biophys Acta* 2008; **1783**: 838-848 [PMID: 18062927 DOI: 10.1016/j.bbamcr.2007.10.012]

9 **Del Re DP**, Amgalan D, Linkermann A, Liu Q, Kitsis RN. Fundamental Mechanisms of Regulated Cell Death and Implications for Heart Disease. *Physiol Rev* 2019; **99**: 1765-1817 [PMID: 31364924 DOI: 10.1152/physrev.00022.2018]

10 **Hwang J**, Suh HW, Jeon YH, Hwang E, Nguyen LT, Yeom J, Lee SG, Lee C, Kim KJ, Kang BS, Jeong JO, Oh TK, Choi I, Lee JO, Kim MH. The structural basis for the negative regulation of thioredoxin by thioredoxin-interacting protein. *Nat Commun* 2014; **5**: 2958 [PMID: 24389582 DOI: 10.1038/ncomms3958]

11 **Li Y**, Miao LY, Xiao YL, Huang M, Yu M, Meng K, Cai HR. Hypoxia induced high expression of thioredoxin interacting protein (TXNIP) in non-small cell lung cancer and its prognostic effect. *Asian Pac J Cancer Prev* 2015; **16**: 2953-2958 [PMID: 25854388 DOI: 10.7314/apjcp.2015.16.7.2953]

12 **Zhou R**, Yazdi AS, Menu P, Tschopp J. A role for mitochondria in NLRP3 inflammasome activation. *Nature* 2011; **469**: 221-225 [PMID: 21124315 DOI: 10.1038/nature09663]

13 **Yang C**, Xia W, Liu X, Lin J, Wu A. Role of TXNIP/NLRP3 in sepsis-induced myocardial dysfunction. *Int J Mol Med* 2019; **44**: 417-426 [PMID: 31173172 DOI: 10.3892/ijmm.2019.4232]

14 **Weisberg SP**, McCann D, Desai M, Rosenbaum M, Leibel RL, Ferrante AW Jr. Obesity is associated with macrophage accumulation in adipose tissue. *J Clin Invest* 2003; **112**: 1796-1808 [PMID: 14679176 DOI: 10.1172/JCI19246]

15 **Pruett JE**, Everman SJ, Hoang NH, Salau F, Taylor LC, Edwards KS, Hosler JP, Huffman AM, Romero DG, Yanes Cardozo LL. Mitochondrial function and oxidative stress in white adipose tissue in a rat model of PCOS: effect of SGLT2 inhibition. *Biol Sex Differ* 2022; **13**: 45 [PMID: 35986388 DOI: 10.1186/s13293-022-00455-x]

16 **Chen Y**, Wu Z, Huang S, Wang X, He S, Liu L, Hu Y, Chen L, Chen P, Liu S, He S, Shan B, Zheng L, Duan SZ, Song Z, Jiang L, Wang QA, Gan Z, Song BL, Liu J, Rui L, Shao M, Liu Y. Adipocyte IRE1α promotes PGC1α mRNA decay and restrains adaptive thermogenesis. *Nat Metab* 2022; **4**: 1166-1184 [PMID: 36123394 DOI: 10.1038/s42255-022-00631-8]

17 **Hwang I**, Jo K, Shin KC, Kim JI, Ji Y, Park YJ, Park J, Jeon YG, Ka S, Suk S, Noh HL, Choe SS, Alfadda AA, Kim JK, Kim S, Kim JB. GABA-stimulated adipose-derived stem cells suppress subcutaneous adipose inflammation in obesity. *Proc Natl Acad Sci U S A* 2019; **116**:

11936-11945 [PMID: 31160440 DOI: 10.1073/pnas.1822067116]

18 **Terlecki-Zaniewicz L**, Lämmermann I, Latreille J, Bobbili MR, Pils V, Schosserer M, Weinmüllner R, Dellago H, Skalicky S, Pum D, Almaraz JCH, Scheideler M, Morizot F, Hackl M, Gruber F, Grillari J. Small extracellular vesicles and their miRNA cargo are anti-apoptotic members of the senescence-associated secretory phenotype. *Aging (Albany NY)* 2018; **10**: 1103-1132 [PMID: 29779019 DOI: 10.18632/aging.101452]

19 **Harrell CR**, Jovicic N, Djonov V, Arsenijevic N, Volarevic V. Mesenchymal Stem Cell-Derived Exosomes and Other Extracellular Vesicles as New Remedies in the Therapy of Inflammatory Diseases. *Cells* 2019; **8** [PMID: 31835680 DOI: 10.3390/cells8121605]

20 **van Niel G**, D'Angelo G, Raposo G. Shedding light on the cell biology of extracellular vesicles. *Nat Rev Mol Cell Biol* 2018; **19**: 213-228 [PMID: 29339798 DOI: 10.1038/nrm.2017.125]

21 **Mathieu M**, Martin-Jaular L, Lavieu G, Théry C. Specificities of secretion and uptake of exosomes and other extracellular vesicles for cell-to-cell communication. *Nat Cell Biol* 2019; **21**: 9-17 [PMID: 30602770 DOI: 10.1038/s41556-018-0250-9]

22 **McLellan MA**, Rosenthal NA, Pinto AR. Cre-loxP-Mediated Recombination: General Principles and Experimental Considerations. *Curr Protoc Mouse Biol* 2017; **7**: 1-12 [PMID: 28252198 DOI: 10.1002/cpmo.22]

23 **Gao E**, Lei YH, Shang X, Huang ZM, Zuo L, Boucher M, Fan Q, Chuprun JK, Ma XL, Koch WJ. A novel and efficient model of coronary artery ligation and myocardial infarction in the mouse. *Circ Res* 2010; **107**: 1445-1453 [PMID: 20966393 DOI: 10.1161/CIRCRESAHA.110.223925]

24 **Shen K**, Wang X, Wang Y, Jia Y, Zhang Y, Wang K, Luo L, Cai W, Li J, Li S, Du Y, Zhang L, Zhang H, Chen Y, Xu C, Zhang J, Wang R, Yang X, Wang Y, Hu D. miR-125b-5p in adipose derived stem cells exosome alleviates pulmonary microvascular endothelial cells ferroptosis *via* Keap1/Nrf2/GPX4 in sepsis lung injury. *Redox Biol* 2023; **62**: 102655 [PMID: 36913799 DOI: 10.1016/j.redox.2023.102655]

25 **Ehler E**, Moore-Morris T, Lange S. Isolation and culture of neonatal mouse cardiomyocytes. *J Vis Exp* 2013 [PMID: 24056408 DOI: 10.3791/50154]

26 **Divakaruni AS**, Jastroch M. A practical guide for the analysis, standardization and interpretation of oxygen consumption measurements. *Nat Metab* 2022; **4**: 978-994 [PMID: 35971004 DOI: 10.1038/s42255-022-00619-4]

27 **Zhang T**, Deng W, Deng Y, Liu Y, Xiao S, Luo Y, Xiang W, He Q. Mechanisms of ferroptosis regulating oxidative stress and energy metabolism in myocardial ischemia-reperfusion injury and a novel perspective of natural plant active ingredients for its treatment. *Biomed Pharmacother* 2023; **165**: 114706 [PMID: 37400352 DOI: 10.1016/j.biopha.2023.114706]

28 **Sluijter JPG**, Davidson SM, Boulanger CM, Buzás EI, de Kleijn DPV, Engel FB, Giricz Z, Hausenloy DJ, Kishore R, Lecour S, Leor J, Madonna R, Perrino C, Prunier F, Sahoo S, Schiffelers RM, Schulz R, Van Laake LW, Ytrehus K, Ferdinandy P. Extracellular vesicles in diagnostics and therapy of the ischaemic heart: Position Paper from the Working Group on Cellular Biology of the Heart of the European Society of Cardiology. *Cardiovasc Res* 2018; **114**: 19-34 [PMID: 29106545 DOI: 10.1093/cvr/cvx211]

29 **Boulanger CM**, Loyer X, Rautou PE, Amabile N. Extracellular vesicles in coronary artery disease. *Nat Rev Cardiol* 2017; **14**: 259-272 [PMID: 28150804 DOI: 10.1038/nrcardio.2017.7]

30 **Lener T**, Gimona M, Aigner L, Börger V, Buzas E, Camussi G, Chaput N, Chatterjee D, Court FA, Del Portillo HA, O'Driscoll L, Fais S, Falcon-Perez JM, Felderhoff-Mueser U, Fraile L, Gho YS, Görgens A, Gupta RC, Hendrix A, Hermann DM, Hill AF, Hochberg F, Horn PA, de Kleijn D, Kordelas L, Kramer BW, Krämer-Albers EM, Laner-Plamberger S, Laitinen S, Leonardi T, Lorenowicz MJ, Lim SK, Lötvall J, Maguire CA, Marcilla A, Nazarenko I, Ochiya T, Patel T, Pedersen S, Pocsfalvi G, Pluchino S, Quesenberry P, Reischl IG, Rivera FJ, Sanzenbacher R, Schallmoser K, Slaper-Cortenbach I, Strunk D, Tonn T, Vader P, van Balkom BW, Wauben M, Andaloussi SE, Théry C, Rohde E, Giebel B. Applying extracellular vesicles based therapeutics in clinical trials - an ISEV position paper. *J Extracell Vesicles* 2015; **4**: 30087 [PMID: 26725829 DOI: 10.3402/jev.v4.30087]

31 **Elsharkasy OM**, Nordin JZ, Hagey DW, de Jong OG, Schiffelers RM, Andaloussi SE, Vader P. Extracellular vesicles as drug delivery systems: Why and how? *Adv Drug Deliv Rev* 2020; **159**: 332-343 [PMID: 32305351 DOI: 10.1016/j.addr.2020.04.004]

32 **Tran TT**, Kahn CR. Transplantation of adipose tissue and stem cells: role in metabolism and disease. *Nat Rev Endocrinol* 2010; **6**: 195-213 [PMID: 20195269 DOI: 10.1038/nrendo.2010.20]

33 **Kranendonk ME**, Visseren FL, van Balkom BW, Nolte-'t Hoen EN, van Herwaarden JA, de Jager W, Schipper HS, Brenkman AB, Verhaar MC, Wauben MH, Kalkhoven E. Human adipocyte extracellular vesicles in reciprocal signaling between adipocytes and macrophages. *Obesity (Silver Spring)* 2014; **22**: 1296-1308 [PMID: 24339422 DOI: 10.1002/oby.20679]

34 **Park H**, Ryu K, Kim YH, Choi WJ, Ko D. The effects of etomidate and midazolam on adipose tissue-derived mesenchymal stem cell proliferation. *Korean J Anesthesiol* 2016; **69**: 614-618 [PMID: 27924203 DOI: 10.4097/kjae.2016.69.6.614]

35 **Park HS**, Song JW, Park JH, Lim BK, Moon OS, Son HY, Lee JH, Gao B, Won YS, Kwon HJ. TXNIP/VDUP1 attenuates steatohepatitis *via* autophagy and fatty acid oxidation. *Autophagy* 2021; **17**: 2549-2564 [PMID: 33190588 DOI: 10.1080/15548627.2020.1834711]

36 **Li N**, Zhou H, Wu H, Wu Q, Duan M, Deng W, Tang Q. STING-IRF3 contributes to lipopolysaccharide-induced cardiac dysfunction, inflammation, apoptosis and pyroptosis by activating NLRP3. *Redox Biol* 2019; **24**: 101215 [PMID: 31121492 DOI: 10.1016/j.redox.2019.101215]

37 **Lv H**, Zhu C, Wei W, Lv X, Yu Q, Deng X, Ci X. Enhanced Keap1-Nrf2/Trx-1 axis by daphnetin protects against oxidative stress-driven hepatotoxicity *via* inhibiting ASK1/JNK and Txnip/NLRP3 inflammasome activation. *Phytomedicine* 2020; **71**: 153241 [PMID: 32454347 DOI: 10.1016/j.phymed.2020.153241]

38 **Park SJ**, Kim Y, Li C, Suh J, Sivapackiam J, Goncalves TM, Jarad G, Zhao G, Urano F, Sharma V, Chen YM. Blocking CHOP-dependent TXNIP shuttling to mitochondria attenuates albuminuria and mitigates kidney injury in nephrotic syndrome. *Proc Natl Acad Sci U S A* 2022; **119**: e2116505119 [PMID: 35994650 DOI: 10.1073/pnas.2116505119]

39 **Mao C**, Li D, Zhou E, Gao E, Zhang T, Sun S, Gao L, Fan Y, Wang C. Extracellular vesicles from anoxia preconditioned mesenchymal stem cells alleviate myocardial ischemia/reperfusion injury. *Aging (Albany NY)* 2021; **13**: 6156-6170 [PMID: 33578393 DOI: 10.18632/aging.202611]

40 **Wang J**, Li L, Zhang Z, Zhang X, Zhu Y, Zhang C, Bi Y. Extracellular vesicles mediate the communication of adipose tissue with brain and promote cognitive impairment associated with insulin resistance. *Cell Metab* 2022; **34**: 1264-1279.e8 [PMID: 36070680 DOI: 10.1016/j.cmet.2022.08.004]

41 **Michel LYM**. Extracellular Vesicles in Adipose Tissue Communication with the Healthy and Pathological Heart. *Int J Mol Sci* 2023; **24** [PMID: 37175451 DOI: 10.3390/ijms24097745]

42 **Wei M**, Gao X, Liu L, Li Z, Wan Z, Dong Y, Chen X, Niu Y, Zhang J, Yang G. Visceral Adipose Tissue Derived Exosomes Exacerbate Colitis Severity *via* Pro-inflammatory MiRNAs in High Fat Diet Fed Mice. *ACS Nano* 2020; **14**: 5099-5110 [PMID: 32275391 DOI:

10.1021/acsnano.0c01860]

43 **Farrell MR**, Rogers LK, Liu Y, Welty SE, Tipple TE. Thioredoxin-interacting protein inhibits hypoxia-inducible factor transcriptional activity. *Free Radic Biol Med* 2010; **49**: 1361-1367 [PMID: 20692333 DOI: 10.1016/j.freeradbiomed.2010.07.016]

44 **O'Gara PT**, Kushner FG, Ascheim DD, Casey DE Jr, Chung MK, de Lemos JA, Ettinger SM, Fang JC, Fesmire FM, Franklin BA, Granger CB, Krumholz HM, Linderbaum JA, Morrow DA, Newby LK, Ornato JP, Ou N, Radford MJ, Tamis-Holland JE, Tommaso CL, Tracy CM, Woo YJ, Zhao DX, Anderson JL, Jacobs AK, Halperin JL, Albert NM, Brindis RG, Creager MA, DeMets D, Guyton RA, Hochman JS, Kovacs RJ, Kushner FG, Ohman EM, Stevenson WG, Yancy CW; American College of Cardiology Foundation/American Heart Association Task Force on Practice Guidelines. 2013 ACCF/AHA guideline for the management of ST-elevation myocardial infarction: a report of the American College of Cardiology Foundation/American Heart Association Task Force on Practice Guidelines. *Circulation* 2013; **127**: e362-e425 [PMID: 23247304 DOI: 10.1161/CIR.0b013e3182742cf6]

Published by **Baishideng Publishing Group Inc**
7041 Koll Center Parkway, Suite 160, Pleasanton, CA 94566, USA
Telephone: +1-925-3991568
E-mail: office@baishideng.com
Help Desk: https://www.f6publishing.com/helpdesk
https://www.wjgnet.com